Salt melt induced corrosion of metallic materials in waste incineration plants

Salzschmelzeninduzierte Korrosion metallischer Werkstoffe in Müllverbrennungsanlagen

M. Spiegel*

This paper presents the analysis of corrosion damages of metallic materials after application in waste fired boilers. The first part gives a description of corroded metallic specimens, collected from different grate fired plants in Germany and it will provide the base information for thermodynamic calculations and laboratory experiments, described in the second part of the paper.

In deposits from boiler tubes of waste incinerators there are significant amounts of molten phases, consisting of calcium-, potassium- and sodium-sulfates and/or potassium- and sodium-chlorides containing heavy-metals like lead and zinc. These heavy-metals are decreasing the melting point of the deposits and severe corrosion occurs especially by the molten phase. A thermodynamic approach is given which describes the stability of chlorides with respect to sulfates in deposits from waste fired boilers. It is shown that in HCl-containing gases especially heavy-metal sulfates will react to corresponding volatile chlorides. In addition, laboratory experiments are presented on the effect of heavy-metal sulfates and chlorides in the corrosion of several metallic materials. The experiments were carried out beneath a $CaSO_4$-K_2SO_4-Na_2SO_4-$ZnSO_4$-$PbSO_4$ salt mixture at 600 °C, beneath the heavy-metal chlorides $PbCl_2$, $ZnCl_2$ and also beneath a $ZnCl_2$-KCl mixture at 300–600 °C. The results of these studies show clearly the strong corrosive effect of heavy-metal rich salt mixtures in the corrosion of steels and nickel-based alloys.

Die vorliegende Veröffentlichung stellt Korrosionserscheinungen an metallischen Werkstoffen aus Müllverbrennungsanlagen vor. Im ersten Teil wird ausführlich auf die Untersuchung korrodierter Werkstoffe aus deutschen Müllverbrennungsanlagen mit Rostfeuerung eingegangen. Die Ergebnisse dieser Untersuchungen liefern die Grundlage für die im zweiten Teil vorgestellten thermodynamischen Berechnungen und experimentellen Studien.

In den Ablagerungen der Überhitzerrohre aus Müllverbrennungsanlagen bilden sich signifikante Mengen geschmolzener Salze. Diese entstehen zum einen aus Sulfaten des Calziums, Kaliums und des Natriums und/oder Chloriden hauptsächlich des Kaliums und des Natriums, denen in allen Fällen noch Schwermetallchloride wie $PbCl_2$ und $ZnCl_2$ beigemengt sind. Diese Chloride senken den Schmelzpunkt von Anteilen der Beläge deutlich ab, so daß es zur verstärkten Korrosion durch geschmolzene Salze kommt. Thermodynamische Berechnungen dienen zur Beschreibung relevanter Chlorid-/Sulfatgleichgewichte in Ablagerungen aus Müllverbrennungsanlagen. Dabei wird gezeigt, daß speziell Schwermetallsulfate in HCl-haltiger Atmosphäre zu entsprechenden gasförmigen Chloriden umgesetzt werden können. Desweiteren wurden Laborexperimente an unterschiedlichen metallischen Werkstoffen durchgeführt, um die Wirkung von Schwermetallsulfaten und -chloriden auf metallische Werkstoffe genauer zu studieren. Die Experimente wurden durchgeführt unter einer $CaSO_4$-K_2SO_4-Na_2SO_4-$ZnSO_4$-$PbSO_4$-Salzmischung bei 600 °C sowie unter den Schwermetallchloriden $PbCl_2$, $ZnCl_2$ und einer $ZnCl_2$-KCl-Salzmischung bei 300–600 °C. Die Ergebnisse der Untersuchungen belegen deutlich den starken korrosiven Effekt schwermetallhaltiger Salzschmelzen auf Stähle und Nickelbasiswerkstoffe.

1 Introduction

One of the most important problems of the civilized society is the removal of waste, mainly stemming from the production of highly developed industrial products. An effective and useful way of removal is the combustion, connected with the production of steam in order to produce electrical energy. Nowadays approximately 23% of the total amount of waste in Europe is burned, whereas the rest is deposited in landfills [1]. In Western Europe, nearly 600 plants are in operation and the number is still increasing.

The process of burning waste produces very corrosive combustion products, due to the complex and heterogeneous composition of the fuel. Especially the increasing amount of chlorine containing compounds such as PVC and the restrictions of the 17 BImSchV in Germany, demanding higher temperatures of combustions, have caused severe corrosion problems in waste fired boilers. Table 1 gives data on the concentrations of some corrosive components in the flue gas of waste fired boilers [2]. Especially HCl and SO_2 are present, and the amount of HCl is significantly higher than those of SO_2. The estimated amount of chlorine from PVC in municiple solid waste in the US based on an analysis by *Wright* et al. [3] will increase from about 0.1% Cl at 1960 to about 1.6% in the year 2000. Table 2 shows amounts of heavy-metals and also of chlorine in deposits of three different plants in Germany, analysed by the author. The tables show quite clearly that heavy-metals are present in deposits in significant amounts, in addition to chlorine. Especially heavy-metal chlorides, but also sulfates are forming low melting eutectics within the deposits so that the occurrence of molten phases is

* Dr. *M. Spiegel*,
Max-Planck-Institut für Eisenforschung GmbH,
Max-Planck-Str. 1, 40237 Düsseldorf (Germany)

 0947-5117/99/0707-0373$17.50+.50/0

Table 1. Corrosive gas species in waste fired boilers [2]. Especially the amount of HCl is generally high, whereas the concentration of SO_2 is in general lower than those of HCl

Tabelle 1. Korrosive Gasspecies in Müllverbrennungsanlagen [2]. Es treten insbesondere hohe Gehalte an HCl auf. Die Konzentration an SO_2 ist im allgemeinen niedriger als die von HCl

Species	Concentration (vppm)
HCl	560–2240
SO_2	100–2000
SO_3	1.4–19.6
NO_2	71.5–214.5
CO	64–640

Table 2. Heavy-metal contents (Pb and Zn) and concentrations of choride (wt.%) in deposits from three different waste boilers in Germany

Tabelle 2. Schwermetallgehalte (Pb und Zn) sowie Chloridkonzentrationen in Ablagerungen dreier unterschiedlicher deutscher Müllverbrennungsanlagen

	Pb^{2+}	Zn^{2+}	Cl^-
deposit 1	7.4	2.3	0.5
deposit 2	1.6	2.9	0.1
deposit 3	7.5	9.7	1.2

most probable. Table 3 gives an overview of some of those low melting salt mixtures (partially extracted from [4]).

Analysis of corrosion phenomena and also laboratory corrosion studies under waste incineration conditions were carried out since many years. A lot of work was done by *Krause* and coworkers from the Battelle Institute in the United States. Systematic studies on the effect of chlorine content in the waste on the corrosion of carbon steel were conducted in the temperature range from 204 to 538 °C. It was found that addition of PVC to the waste increases the chlorine content in the deposits and, therefore, the corrosion rate of the steel is enhanced by a factor from 50–150% [5]. From these experiments, the more corrosive effect of chlorides in the deposits with respect to the sulfates was seen. Several reactions were put forward by *Vaughan* et al. [6], involving chlorine and sulfur species, partially releasing HCl or Cl_2 or forming solid NaCl as reaction products.

Reese and *Grabke* [7, 8] have shown the corrosive effect of solid chlorides like KCl, NaCl, $MgCl_2$ and $CaCl_2$ on low- and high alloy steels in He-O_2 and He-O_2-SO_2-atmospheres at 500 and 700 °C by thermogravimetric experiments. The salt reacts with the oxide scale of the preoxidized sample forming ferrate or chromate and releasing chlorine:

$$NaCl + Fe_2O_3 + 1/2\ O_2 = NaFe_2O_4 + 1/2\ Cl_2 \quad (1)$$

$$2\ NaCl + Cr_2O_3 + 5/2\ O_2 = 2\ NaCrO_4 + Cl_2 \quad (2)$$

The chlorine diffuses through cracks and pores of the oxide scale to the metal/scale interface, reacting to $FeCl_2$(s):

$$Fe + Cl_2 = FeCl_2(s) \quad (3)$$

As the vapour pressure of the chloride is 10^{-4} bar at 500 °C, it evaporates and the volatile chloride diffuses outward through the oxide scale. At the interface oxide/gas atmosphere the reaction to Fe_2O_3 takes place and releasing chlorine again:

$$2\ FeCl_2(g) + 3/2\ O_2 = Fe_2O_3 + 2\ Cl_2 \quad (4)$$

The growth of the Fe_2O_3 in cracks and pores of the oxide destroys the scale and corrosive gas can react with the unprotected metal. Hence, a scale is produced on the metal substrate which is not passivating and for this reason, the mechanism was nominated active oxidation by *Lee* and *McNallan* [9]. The chlorine plays a catalytic role in this corrosion process, because it is not consumed. In depth thermogravimetric studies on the mechanism of active oxidation were carried out by *Reese* and *Grabke* [7], showing that evaporation of $FeCl_2$(g) from the metal/scale interface is the rate determining step in NaCl induced corrosion.

Further work with fly ash deposits from waste incinerator plants was carried out by *Spiegel* and *Grabke* [10–12], using thermogravimetric experiments and exposure tests. Deposition of fly ash deposits on the 2.25Cr-1Mo steel leads to enhanced corrosion at 500 °C in He-O_2 atmospheres due to chlorides, present in the deposits [10, 11]. The corrosion was severe in He-O_2-HCl atmospheres due to the formation of alkali- and heavy-metal chlorides in the deposits by reaction of sulfates with HCl gas:

$$(K,\ Na)_2Ca_2(SO_4)_3 + 2\ HCl = 2\ (K,\ Na)Cl + 2\ CaSO_4 + SO_2 + H_2O + 1/2\ O_2 \quad (5)$$

Addition of SO_2 to the He-O_2-HCl mixture leads to decreased corrosion due to the stabilization of the sulfates in the deposits. In exposure tests on high alloy steels at 600 °C in N_2-O_2, a molten sulfate/chloride phase was observed in the deposits [12] and heavy-metal rich corrosion products like $PbCrO_4$ and $ZnCr_2O_4$ were observed on top of the oxide scale beneath the deposits. The corrosion process

Table 3. Melting points of salt mixtures containing heavy-metal compounds. Especially the chlorides have low melting points down to 250 °C

Tabelle 3. Schmelzpunkte schwermetallhaltiger Salzmischungen. Insbesondere die Schmelzpunkte der Chloridmischungen sinken bis zu 250 °C

composition [wt.%]	melting point [°C]
$ZnCl_2$	318
$PbCl_2$	498
48$ZnCl_2$-52 KCl	250
82$ZnCl_2$-18 KCl	262
84$ZnCl_2$-16 KCl	262
73$ZnCl_2$-27$PbCl_2$	300
31NaCl-69$PbCl_2$	410
21KCl-79$PbCl_2$	411
17NaCl-83$PbCl_2$	415
39$ZnCl_2$-50KCl-11$PbCl_2$	275
35$ZnCl_2$-48NaCl-17$PbCl_2$	350
16NaCl-40KCl-44 $PbCl_2$	400
K_2SO_4-Na_2SO_4-$ZnSO_4$	384
KCl-$ZnCl_2$-K_2SO_4-$ZnSO_4$	292
K_2SO_4-Na_2SO_4-$CaSO_4$	776

was recognized basic fluxing by a heavy-metal rich salt melt. In N_2-O_2-SO_2, acidic fluxing takes place and the corrosive attack is less severe. These experiments show quite clearly the inhibiting effect of SO_2 on chlorine induced corrosion beneath fly ash deposits.

Studies on the effect of molten phases in deposits on the corrosion of steels were carried out especially in the United States and also in Japan. *Otsuka* et al. [13] studied the effect of a KCl-NaCl-$FeCl_2$ mixture with additions up to 30 mol.% $PbCl_2$ on the corrosion of steels and nickel-based alloys in the atmosphere N_2 – 20 vol.% H_2O – 7.5 vol.% O_2 – 7.5 vol.% CO with 1500 vppm HCl – 300 vppm SO_2. They observed enhanced corrosion already at 400 °C, and the extent of attack decreases with increasing nickel content of the alloy. Compared with a deposit containing chloride, application of a Na_2SO_4-K_2SO_4 mixture below its melting point not significantly affects on the corrosion of the tested alloys in the same gas atmosphere. Further investigations on this topic were carried out by *Kawahara* et al. [14]. They studied the effect of additions of $PbCl_2$, $ZnCl_2$ and $ZnSO_4$ to a waste incinerator ash on the corrosion of steels and coating materials like 80Ni20Cr. The experiments were carried out at 350 and 230 °C in an N_2 – 20 vol.% O_2 – 10 vol.% CO_2 – 10 vol.% O_2 – atmosphere with addition of 1000 vppm HCl and 100 vppm SO_2. After addition of $PbCl_2$ and $ZnCl_2$, enhanced corrosion of the materials was observed, whereas after addition of $ZnSO_4$ the corrosion decreases compared to the unmodified ash.

2 Analysis of corroded specimens

This chapter gives an overview of corroded sample analysis from waste incinerator plants, carried out at the MPI für Eisenforschung in Düsseldorf. The samples were taken from three different plants in Germany and they have been in service for thousands of hours. The analysis shows quite clearly the occurrence of a molten phase in the deposits, found on the surface of the tubes. The melt consists of sulfates and/or chlorides and contains significant amounts of zinc and also lead to a much smaller extent.

2.1 Analysis No. 1

The analysed specimen is a tube made of 15 Mo 3, overlayed with a nickel based alloy as shown in Fig. 1. The chemical analysis of the alloy is given in Table 4. At the part directly exposed to the gas flow, the overlay was covered with a thick layer of deposits and complete consumption has taken place by corrosion after 6000 h of exposure. It is important to note that at the left and right hand side of the tube and also at the back there are only small amounts of deposits and, therefore, the corrosion was found to be much less.

Table 4. EDX-analysis (wt.%) of the corroded overlay on 15 Mo 3. It is a nickel-based alloy, containing 4.6 wt.% of silicon

Tabelle 4. EDX-Analyse (Gew.%) der korrodierten Beschichtung auf 15 Mo 3. Es handelt sich um eine Nickelbasislegierung mit 4,6 Gew.% Silizium

Ni	Cr	Fe	Si
70.6	16.7	8.1	4.6

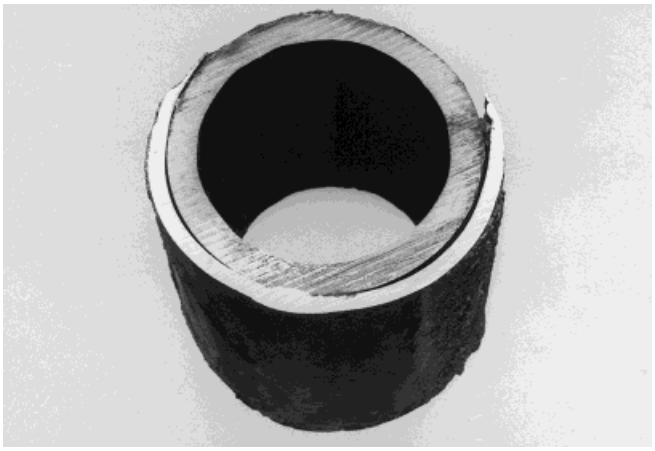

Fig. 1. Corrosion damage of a nickel based overlay on a tube of 15 Mo 3 (see Table 4 for chemical analysis). In direct contact with the flowing gas, the tube was covered with a thick layer of deposits and the overlay is completely destroyed by corrosion. The left and right hand side and also the back were not in direct contact with the gas stream and, therefore, only small amounts of deposits are found and the corrosion is much less in this area

Abb. 1. Korrosionsschäden einer Nickelbasisbeschichtung aufgebracht auf einem Rohr aus 15 Mo 3 (chemische Analyse siehe Tabelle 4). In direktem Kontakt mit dem Rauchgas (Anströmkante) war das Rohr mit dicken Belägen bedeckt, an dieser Stelle ist die Beschichtung komplett durch Korrosion aufgezehrt. Die linke und rechte Seite des Rohres als auch die Rückseite waren nicht direkt von Rauchgas angeströmt, es finden sich daher weniger Beläge und folglich auch eine deutlich geringere Korrosion

2.1.1 Analysis of the deposits

In order to examine the reason for the damage of the overlay, analysis of the deposits was carried out by SEM on the heavy corroded part of the tube (front side) and also on the left and right hand side, as well at the contact area deposits/gas and at the interface deposits/oxide. A SEM-micrograph of the deposit/gas interface from the front side of the tube (Fig. 2a), shows a solidified molten phase beneath solid particles. The result of the EDX-analysis of the molten phase is given in Fig. 2b. The melt contains sulfur, oxygen, small amounts of chlorine, furthermore potassium, sodium, calcium as well as lead and small amounts of zinc. Obviously, a sulfate melt containing heavy-metals and small amounts of chlorine has been formed in contact with the flue gas. A SEM-micrograph of the same deposits, taken at the oxide/deposit interface is shown in Fig. 3a. Also in this case, a solidified molten phase was detected, the results of its EDX-analysis are shown in Fig. 3b. In contrast to the melt at the gas/deposits interface this melt consists of potassium, zinc and chlorine and no sulfur and no oxygen were detected, it is obviously a $ZnCl_2$-KCl eutectic. In the deposits from the back and also from the left and right hand side of the tube no significant amounts of chlorine and no molten phases were detected. These deposits mainly consist of sulfates of calcium, potassium and lead. In conclusion, the severe corrosion of the overlay alloy occurs beneath chlorine containing deposits, showing a significant amount of molten phase (sulfates and chlorides) containing heavy-metals like lead and zinc.

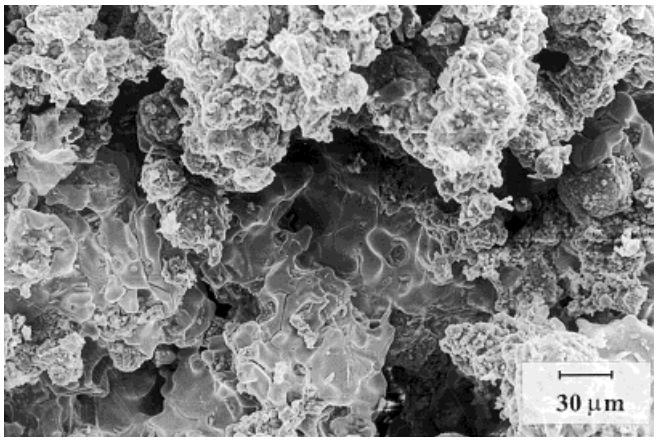

Fig. 2a. SEM-micrograph of the deposits from the heavily corroded part of the tube (front part). The picture represents the contact area between the deposit and the flue gas, showing a molten phase

Abb. 2a. REM-Abbildung der Beläge aus dem korrodierten Bereich des Rohres (Vorderseite). Das Bild zeigt die Kontaktfläche zwischen Ablagerungen und Rauchgas. Deutlich zu erkennen ist die Schmelzphase

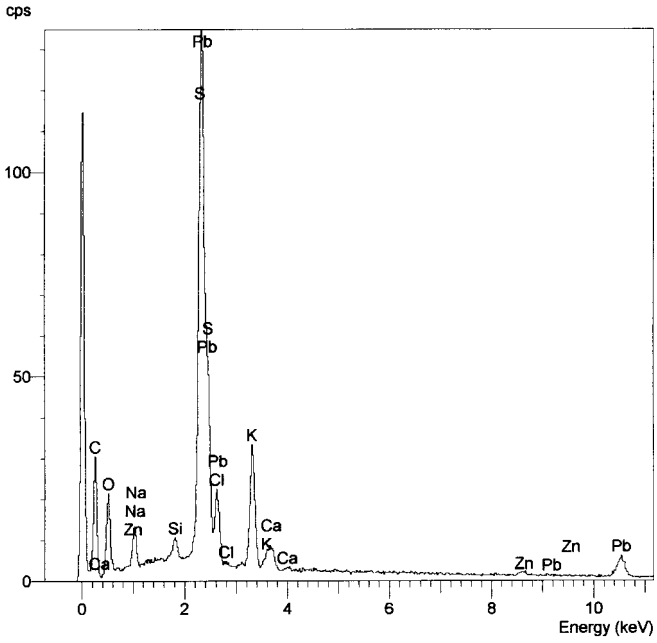

Fig. 2b. EDX-analysis of the melt from Fig. 2a, containing high amounts of sulfur, some oxygen and chlorine besides potassium, calcium and sodium, the heavy-metals lead and small amounts of zinc are present

Abb. 2b. EDX-Analyse der Schmelze aus Abb. 2a. Die Schmelze enthält hohe Gehalte an Schwefel, etwas Sauerstoff und Chlor in Verbindung mit Kalium, Calzium und Natrium. Als Schwermetalle sind Blei und wenig Zink nachzuweisen

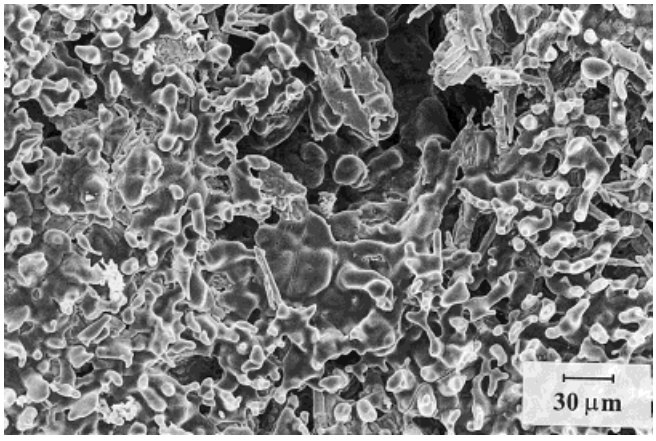

Fig. 3a. SEM-micrograph of the deposits from the heavily corroded part of the tube (front part). The picture represents the contact area between the deposit and the oxide scale, formed on the metal. Also in this position a molten phase has formed

Abb. 3a. REM-Abbildung der Beläge aus dem korrodierten Bereich des Rohres (Vorderseite). Das Bild zeigt die Kontaktfläche zwischen Ablagerungen und Oxidschicht auf dem Metall. Auch an dieser Stelle ist Schmelzphase zu finden

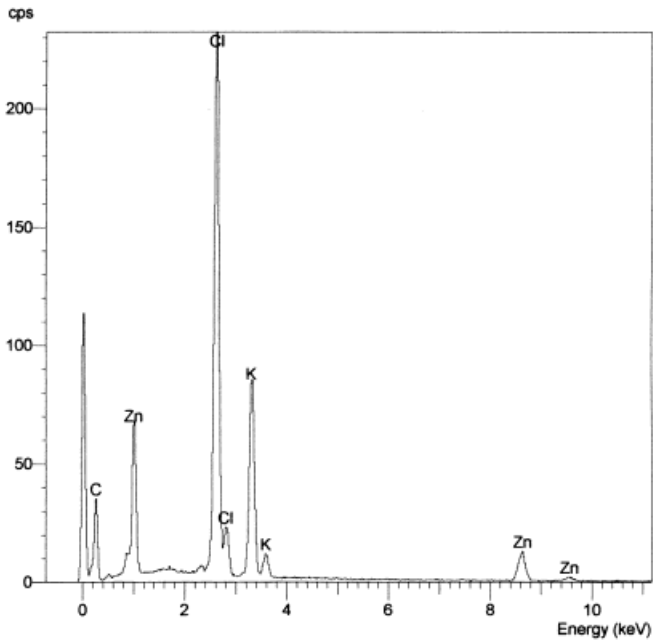

Fig. 3b. EDX-analysis of the melt from Fig. 3a: In contrast to the melt at the deposit/gas interface mainly chlorine and no sulfur and oxygen is detected. The melt consists of $ZnCl_2$-KCl

Abb. 3b. EDX-Analyse der Schmelze aus Abb. 3a. Im Gegensatz zur Schmelze an der Phasengrenze Ablagerung/Gas findet sich hier im wesentlichen Chlor. Schwefel und Sauerstoff wurden nicht nachgewiesen. Die Schmelze besteht aus $ZnCl_2$ und KCl

2.1.2 Analysis on corroded metal specimens

Analysis was also carried out on corroded metal specimens from the front of the tube, i.e. alloy 15 Mo 3 and the overlay alloy. On 15 Mo 3 a thick oxide scale consisting of mainly Fe_2O_3 was found, indicating active oxidation. On top of this scale, the $ZnCl_2$-KCl melt was detected. After removal of the oxide, salt was identified on the metal substrate also, mainly chlorides of sodium and potassium, but also sulfates. In some cases, the salt had been molten. Hence, diffusion of volatile salt species, probably molten phases, takes place from the hot flue gas through deposits and cracks

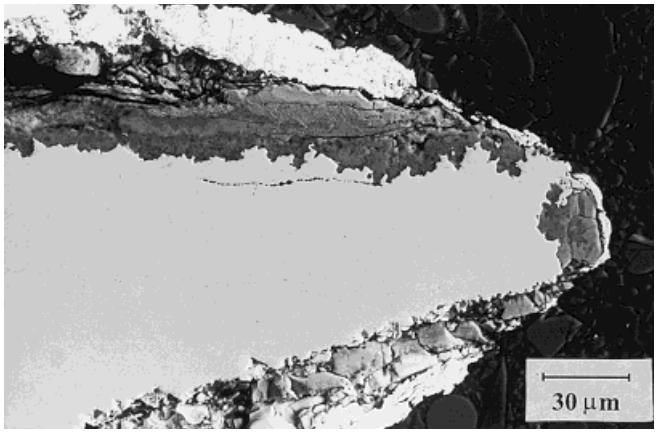

Fig. 4. Corrosion scale on the nickel based overlay. The oxide consists of NiO (bright phase in contact with the gas atmosphere) and spinel (dark phase in contact with the metal)

Abb. 4. Korrosionsschicht auf der Nickelbasislegierung. Das Oxid besteht aus NiO (helle Phase in Kontakt mit der Gasatmosphäre) und Spinell (dunkle Phase in Kontakt mit dem Metall)

and pores of the oxide scale to the metal/scale interface, condensing at the lower temperatures of the metal surface.

In addition, analysis was also carried out on the overlay material. Fig. 4 shows a SEM picture of the overlay from the corrosion front. On the metal, a thick oxide scale has formed, consisting of two different phases. According to the results of X-ray diffraction analysis in combination with EDX, the inner part close to the metal is a spinel and the outer part is NiO. All over the scale, small amounts of sodium and potassium as well as zinc and lead are detected, together with sulfur and chlorine. These results indicates the presence of sulfates and chlorides in the scale. In Fig. 5a, a SEM-magnification of the NiO scale is shown. The picture shows the porous oxide, but also relatively dense layers within the scale. The results of EDX-analysis taken from these parts are given in Fig. 5b. The dense layers are enriched in chromium and also zinc and lead, besides potassium, sulfur and chlorine are detected. The relatively dense morphology and also the composition strongly indicates that these layers had been molten phases, as discussed above. According to the high amout of chromium, a reaction of the melt with an initially formed chromia scale according to:

$$Cr_2O_3 + 4\ KCl + 5/2\ O_2 = 2\ K_2CrO_4 + 2\ Cl_2 \qquad (6)$$

$$Cr_2O_3 + 2\ PbCl_2 + 5/2\ O_2 = 2\ PbCrO_4 + 2\ Cl_2 \qquad (7)$$

$$Cr_2O_3 + ZnCl_2 + 1/2\ O_2 = ZnCr_2O_4 + Cl_2 \qquad (8)$$

may have taken place. On the one hand, the reaction of the melt with Cr_2O_3 scales leads to a depletion of chromium in the alloy and spinel and nickel-oxide can form. On the other hand, chlorine is produced by the reactions (6)–(8). Since the chlorine partial pressures is high enough, metal-chlorides form at the metal scale interface and active oxidation is expected, leading to very high corrosion rates. The actual presence of $FeCl_2$ underneath the oxide scale of the 15 Mo 3 material confirms the mechanism of active oxidation.

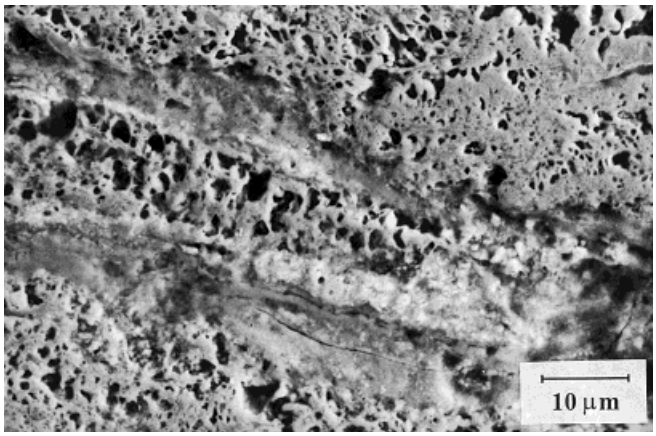

Fig. 5a. SEM-magnification of the NiO-scale in Fig. 4. Within the porous oxide, dense layers are visible

Abb. 5a. REM-Vergrößerung der NiO-Schicht aus Abb. 4. In dem porösen Oxid sind dichtere, bandförmige Einlagerungen zu sehen

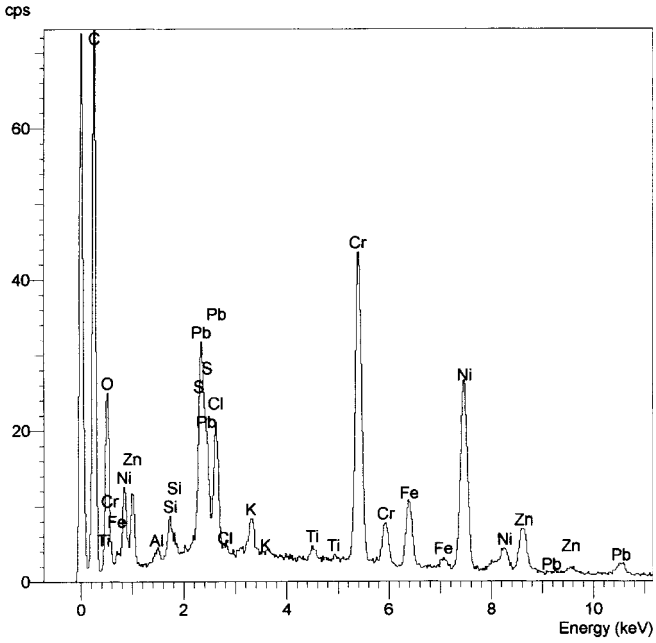

Fig. 5b. EDX-analysis of the dense layers in Fig. 5a. The layers are enriched in chromium, zinc and lead, besides potassium, sulfur and chlorine

Abb. 5b. EDX-Analyse der dichteren Einlagerungen aus Abb. 5a. In diesen Lagen sind Chrom, Zink und Blei neben Kalium, Schwefel und Chlor angereichert

In the beginning of the corrosion process, a chromium-rich oxide layer is formed on the alloy surface. After deposition of fly ash and reaction with the melt in the deposits, this layer is destroyed by reactions (6)–(8) and chromium is depleted in the alloy. In consequence, nickel-rich spinels as well as NiO start to grow and chromium is enriched again. As the nickel-oxide scale is very porous, flue gas and also volatile salts can diffuse to the scale melt interface and condense as solid or molten phases, which attack the metal again. That diffusion of flue gas components through the oxide scale takes place demonstrated above and analysis of the NiO scale strongly indicates that this is possible, since the oxide is sufficiently porous.

Fig. 6. Investigated tube of 15 Mo 3, overwelded with 2.4831 (Inconel 625). Also in this case the overlay is destroyed at the front part of tube, where most of the deposits were found

Abb. 6. Das zu untersuchende Rohr aus 15 Mo 3, auftragsgeschweißt mit dem Werkstoff 2.4831 (Inconel 625). Auch in diesem Fall ist die Beschichtung im vorderen Teil des Rohres durch Korrosion zerstört. In diesem Bereich wurden ebenfalls die meisten Beläge gefunden

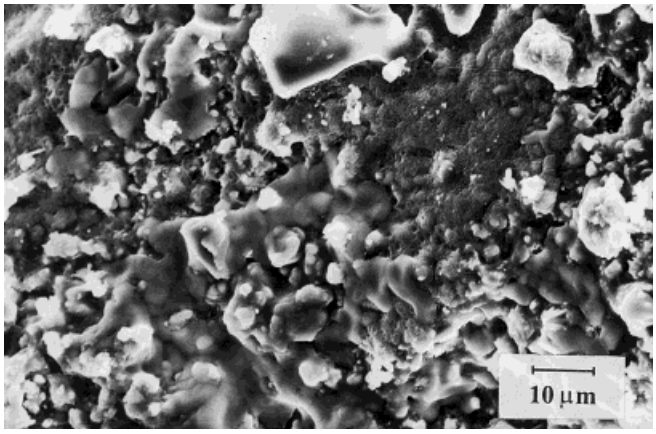

Fig. 7a. SEM-micrograph of the deposits from the front side of the tube (deposit/gas interface). Also in this case a molten phase has formed

Abb. 7a. REM-Abbildung der Ablagerungen von der Vorderseite des Rohres (Grenzfläche Ablagerung/Gas). Auch hier ist Schmelzbildung zu beobachten

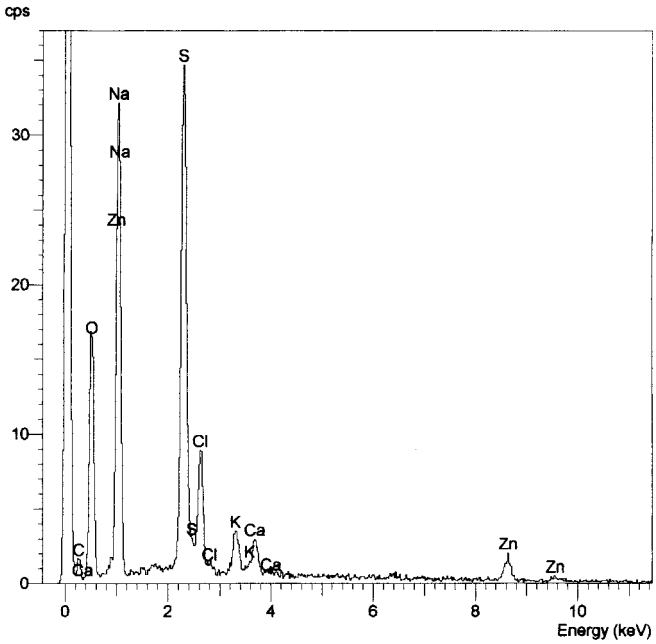

Fig. 7b. EDX-analysis of the melt from Fig. 7a. Besides sulfur, chlorine and oxygen also sodium, potassium, calcium and zinc are identified

Abb. 7b. EDX-Analyse der Schmelzphase aus Abb. 7a. Neben Schwefel, Chlor und Sauerstoff sind hier Natrium, Kalium, Calzium und Zink nachzuweisen

2.2 Analysis No. 2

The analysed specimen was a tube of 15 Mo 3, but in this case overwelded with the nickel-based alloy 2.4831, as shown in Fig. 6. The actual chemical composition of the overlay will be discussed later in more detail. As in the analysis described before, the worst corrosion takes place at the front side of the tube in direct contact with the flue gas, where most of the deposits were found. On the back and also on the left and right hand side there are only small amounts of deposits and less corrosion was observed.

2.2.1 Investigations of deposits

Investigations of deposits from the front side of the tube were carried out, in Fig. 7a a SEM-micrograph of the deposits from the deposit/gas interface is shown. The micrograph shows a solidified molten phase, whereas Fig. 7b its EDX analysis indicates potassium, sodium and calcium and furthermore high amounts of sulfur and oxygen with some chlorine. As a heavy-metal, only zinc is present. According to these results, the melt is a sulfate/chloride mixture, containing a significant amount of zinc and no lead. A SEM-micrograph from deposits of the deposit/scale interface is presented in Fig. 8a, also showing a molten phase, its EDX-analysis is given in Fig. 8b. In comparison with the composition of the deposits/gas interface much chlorine is present, besides sulfur and small amounts of oxygen. It contains mainly potassium and zinc and also some sodium, furthermore iron and also small amount of chromium are dissolved in the melt, whereas nickel was not detected.

For further analysis, metallographic cross sections were prepared from oxide scales with deposits taken from the front part of the tube. In Fig. 9, an overview of the cross section is shown. The outer part in contact with the gas phase of the oxide/deposit system is extremely porous and in contact with the metal much more dense. A magnification of the outer part of the scale is shown in Fig. 10, it shows precipitates within a matrix of a solidified molten phase, consisting mainly of sulfates but also chlorides, as described before. According to EDX-analysis the precipitates are iron- and nickel-oxides, with only small amounts of chromia (Fig. 11). Moving to the metal/scale interface, besides the precipitates also oxide layers are identified, containing iron and nickel and in some cases also chromium. At the scale/metal interface no precipitates are found and the layered oxide contains much more chromium, besides iron and nickel. Fig. 12 shows a mag-

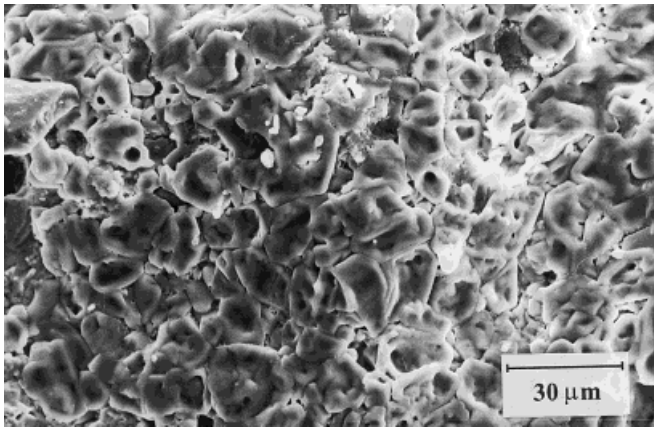

Fig. 8a. SEM-micrograph of the molten phase in the deposits from the front side of the tube (deposit/scale interface)

Abb. 8a. REM-Abbildung der Schmelzphase in den Ablagerungen von der Vorderseite des Rohres (Grenzfläche Ablagerung/Schicht)

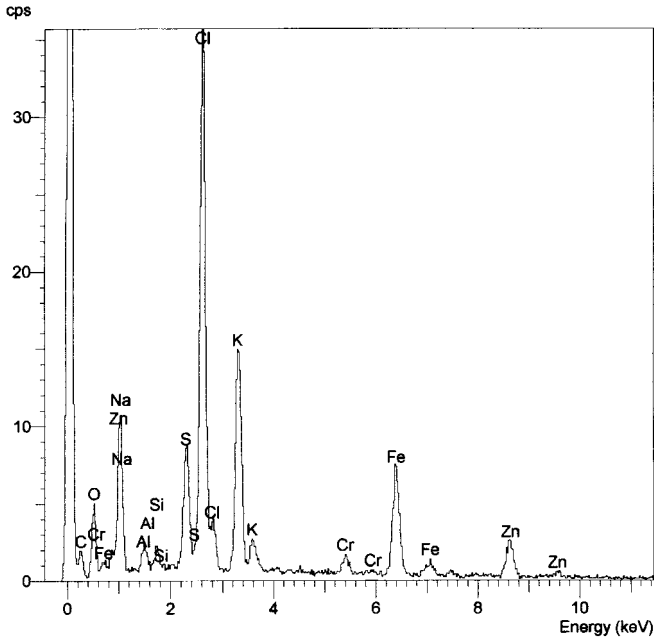

Fig. 8b. EDX-analysis of the melt from Fig. 8a. In comparison with Fig. 7b, less sulfur and more chlorine are detected, besides potassium and zinc. In the melt, also iron and small amounts of chromium are identified. Aluminium and silicon are also detected as deposit material

Abb. 8b. EDX-Analyse der Schmelze aus Abb. 8a. Im Vergleich mit Abb. 7b wurde weniger Schwefel und mehr Chlor, in Verbindung mit Kalium und Zink, nachgewiesen. In der Schmelze finden sich gelöstes Eisen und wenig Chrom. Das Aluminium und Silizium entstammt ebenfalls den Ablagerungen

nification of the inner part of the scale. Within the oxide scale (bright grey), also layers of solidified salt melt (dark grey) were identified, which is in accordance with the observation made in the first analysis.

2.2.2 Investigations of the metallic material

Investigations of the metallic material were carried out, a metallographic cross section of the overweld material is

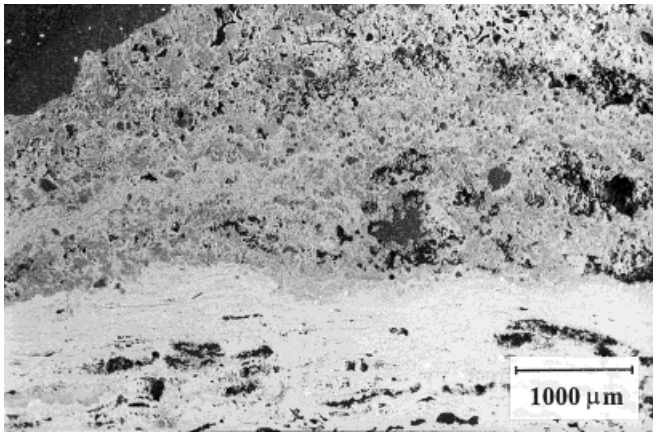

Fig. 9. SEM-micrograph from a metallographic cross section of oxide and deposits, formed in the front area of the tube. The morphology of the oxide is extremely porous in contact with the gas phase and much more dense at the inner part in contact with the metal

Abb. 9. REM-Abbildung eines metallographischen Querschliffs der Oxide und Ablagerungen von der Vorderseite des Rohres. Das Oxid ist extrem porös an der Aussenseite in Kontakt mit der Gasphase und wesentlich dichter im inneren Teil der Schicht in Kontakt mit dem Metall

shown in Fig. 13. The corrosion product intrudes into the metal along dendrites, formed during the welding process. The corrosion product is a mixture of metal-chlorides mainly of iron, chromium and nickel with the corresponding oxides. In addition, also significant amounts of NiS are identified. Considering the high iron content in the product, a quantitative analysis of the overweld material was carried out with EDX (Table 5). Obviously the material has dissolved some iron from the steel substrate during the welding procedure. In addition, the amount of chromium is too low to form protective chromium-rich corrosion products.

The corrosion mechanisms observed in this case, are again mainly due to chlorine, which stems from the chloride-rich melt at the deposit/scale interface. This is indicated by the

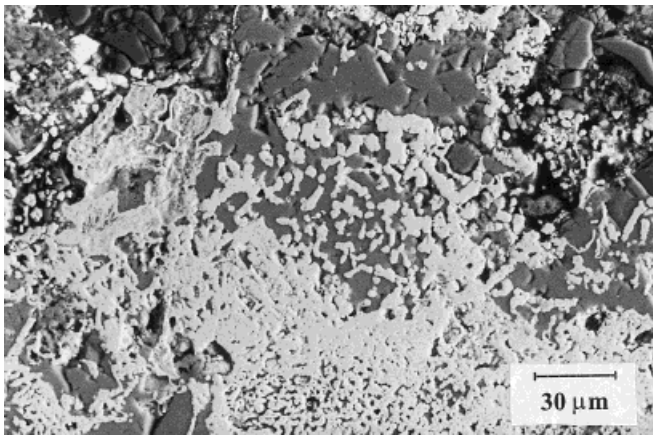

Fig. 10. SEM-magnification of the outer part of the oxide from Fig. 9. The scale consists of oxide precipitates within a matrix of a solidified molten salt (sulfates and chlorides)

Abb. 10. REM-Vergrößerung des äusseren Teils des Oxids aus Abb. 9. Die Schicht besteht aus Ausscheidungen von Oxiden in einer Matrix aus geschmolzenem Salz (Sulfate und Chloride)

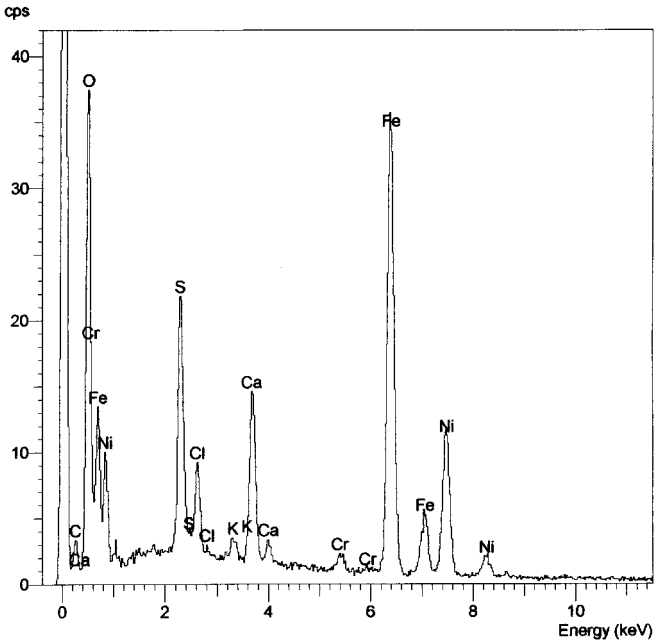

Fig. 11. EDX-analysis of the precipitates in Fig. 10. The oxide contains mainly iron and nickel and only small amounts of chromium

Abb. 11. EDX-Analyse der Ausscheidungen aus Abb. 10. Das Oxid enthält überwiegend Eisen und Nickel aber nur sehr wenig Chrom

formation of metal-chlorides as the main corrosion product. As already described in the first analysis, the melt reacts with the oxide scale to form chlorine, which reacts with the metal to form volatile metal chlorides.

On the other hand, precipitates of iron- and nickel-oxides are observed in the sulfate-rich melt, especially at the deposit/gas interface. This strongly indicates a solubility of iron- and nickel-oxides in the melt, precipitating as oxides during cooling or in contact with oxygen containing gas. Chromia seems

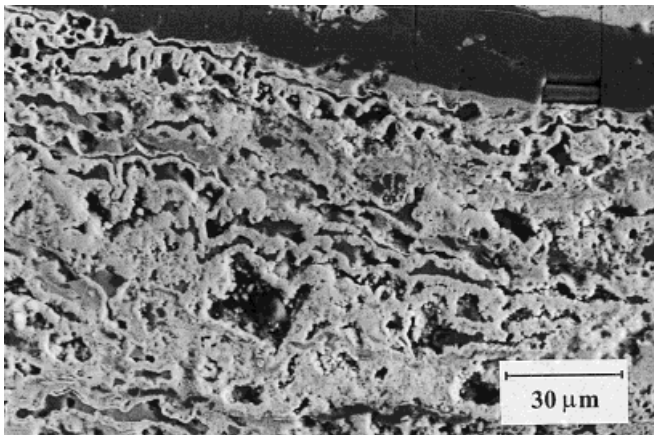

Fig. 12. SEM-magnification of the inner part of the oxide from Fig. 9. The scale is much more dense and consists of layers of chromium-containing iron- and nickel-oxides (bright phase) and solidified salt (dark phase)

Abb. 12. REM-Vergrößerung des inneren Teils der Oxidschicht aus Abb. 9. Die Schicht ist deutlich dichter und besteht aus chromreichem, eisen- und nickelhaltigem Oxid (helle Phase) sowie Einlagerungen von Salz (dunkle Phase)

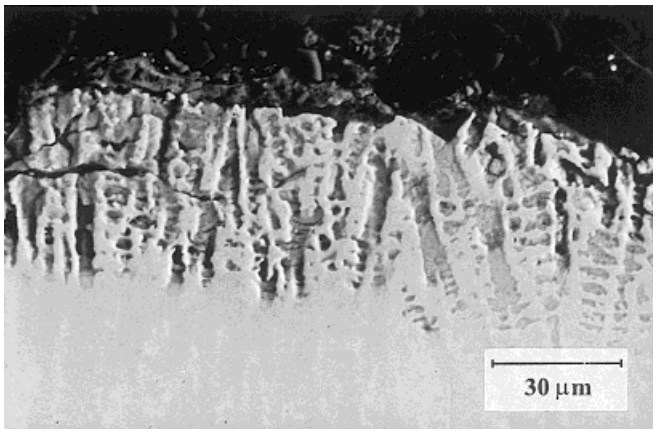

Fig. 13. SEM-image of a metallographic cross section of the overlay material. The corrosion proceeds into the material via the dendritic structure

Abb. 13. REM-Aufnahme eines metallographischen Querschliffs des Beschichtungsmaterials. Die Korrosion schreitet entlang dendritischer Primärausscheidungen in die metallische Matrix fort

to be less soluble, it forms a layered corrosion product underneath these precipitates. Along with the precipitates, also sulfides are formed at the deposit/scale interface, indicating the participitation of the sulfate melt in the corrosion process. In conclusion, corrosion takes place by chlorine produced by reaction of the chloride melt with the oxide scale at the deposit/scale interface and by dissolution of iron- and nickel-oxides in the sulfate melt at the deposits/gas phase boundary along with the formation of nickel-sulfides. This fundamental observation will be discussed in more detail in chapter 3 and 4.

2.3 Analysis No. 3

These studies were conducted on oxides scales with deposits, formed on 15 Mo 3 and St. 35.8 (Table 6). The scales were taken from boiler tubes of a waste incineration plant in Germany. The tubes had been covered with SiC-tiles in order to protect them against corrosion but, obviously, the SiC failed and the flue gas diffused through gaps in the ceramic material to the surface of the tubes and severe corrosion took place. The

Table 5. Chemical composition (mean values) of the overlay as obtained by EDX-analysis (wt.%)

Tabelle 5. Chemische Zusammensetzung (Mittelwerte) des Beschichtungsmaterials (EDX-Analyse, Gew.%)

Ni	Cr	Fe	Mo
53.8	18.4	20.8	7.1

Table 6. Chemical composition of St. 35.8 and 15 Mo 3 (wt.%) [15]

Tabelle 6. Chemische Zusammensetzung von St. 35.8 and 15 Mo 3 (Gew.%) [15]

	Fe	Cr	Si	Mn	Mo
15 Mo 3	bal.	< 0.25	0.1–0.35	0.4–0.9	0.25–0.35
St. 35/8	bal.	–	0.1–0.35	0.4–0.8	–

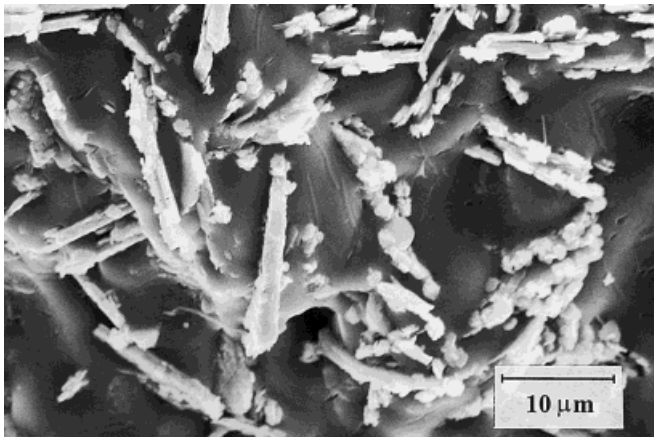

Fig. 14a. Molten phase (sulfate with small amounts of chlorides) on top of the oxide scale of 15 Mo 3. The melt contains precipitates of Fe_2O_3

Abb. 14a. Geschmolzene Phasen (Sulfate, vermengt mit wenig Chloriden) auf der Oberseite der Oxidschicht von 15 Mo 3. Die Schmelze enthält Ausscheidungen von Fe_2O_3

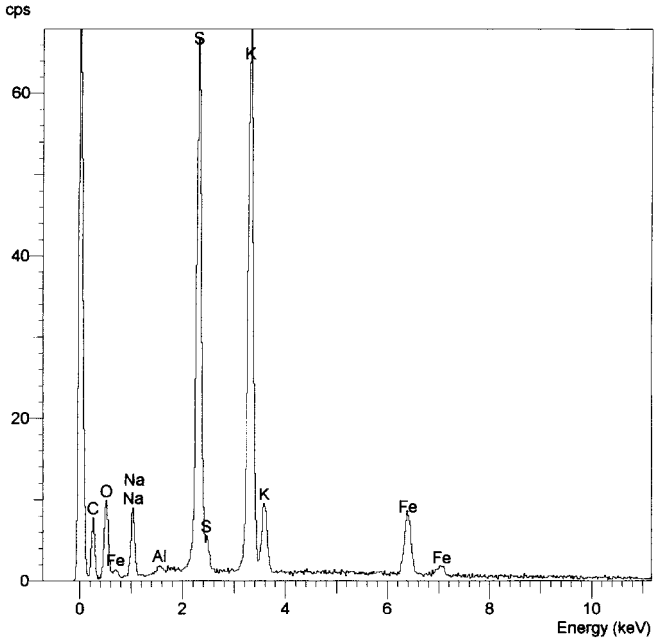

Fig. 14b. EDX-analysis of the melt in Fig. 14a. It is a sulfate melt containing sodium and potassium and some dissolved iron

Abb. 14b. EDX-Analyse der Schmelze aus Abb. 14a. Es handelt sich um eine Sulfatschmelze die Natrium, Kalium sowie gelöstes Eisen enthält

growth of the voluminous corrosion products destroy the ceramic overlay coatings and the corrosion proceeds.

In contact with the SiC material (top of the scale) two kinds of molten phase are observed (Fig. 14a), in wide areas the melt consists of mainly sulfates (potassium, sodium) and dissolved iron (Fig. 14b) but, in some locations, also small amounts of chlorides were detected in the sulfates. On the other hand, a chloride melt was identified on the top of the scale containing zinc- and potassium-chloride with certain amounts of dissolved iron and chromium (Fig. 14c). Fig. 14a also shows precipitates of Fe_2O_3 in the molten sulfate.

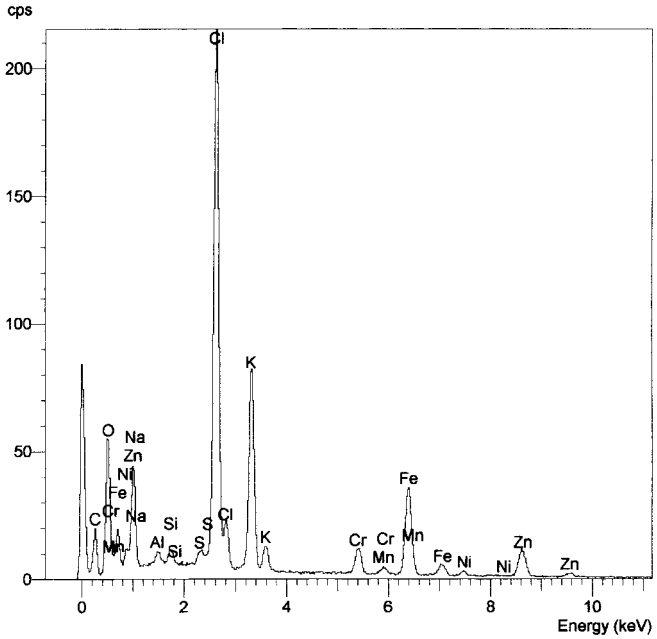

Fig. 14c. EDX-analysis of a melt at another location on top of the oxide. In this case, a KCl-$ZnCl_2$ eutectic was formed

Abb. 14c. EDX-Analyse einer Schmelzphase von anderer Stelle auf der Oberfläche des Oxids. In diesem Fall handelt es sich um eine KCl-$ZnCl_2$-Schmelze

At the metal/scale phase boundary, also a molten phase was detected, which is a sulfate, consisting of potassium, sodium and calcium with some dissolved chlorine. Besides the melt, also crusts of chlorides of sodium and potassium are detected. In contrast to the melt on top of the scale, no dissolved iron was detected.

Investigations of the oxide scales in metallographic cross sections have shown that significant amounts of chlorides (potassium and zinc) are present in the porous oxide scale (Fig. 15). At higher magnifications, precipitates of Fe_2O_3 are observed within the chloride melt (Fig. 16) at the scale/SiC phase boundary. At other locations, also precipitation of porous Fe_2O_3 were observed in the sulfate melt (Fig. 17). The analysis confirms quite clearly the observation of metal oxide precipitates in the sulfate melts, formed in the deposits at the deposit/gas phase boundary.

2.4 Conclusions

The analysis of specimens from waste incinerator plants have shown that severe corrosion of the metallic materials occurs, if a significant amount of deposits containing chlorides and sulfates are present on the surface of the metallic components. In every case which has been analysed a molten phase had formed in the deposits. These molten phases are different in composition, depending on the plant and also depending on the location in the deposits. In general, molten Ca-, K-, Na-sulfates are prevailing at the deposit/gas phase boundary, whereas more molten chlorides ($ZnCl_2$-KCl, NaCl) are present at the deposit/scale phase boundary. Nevertheless, most of the sulfates contain a small amount of chlorides and most of the chlorides contain a small amount of sulfates. The chemistry of the sulfate melt is within the potassium-sodium-calcium-sulfate system, with more or less

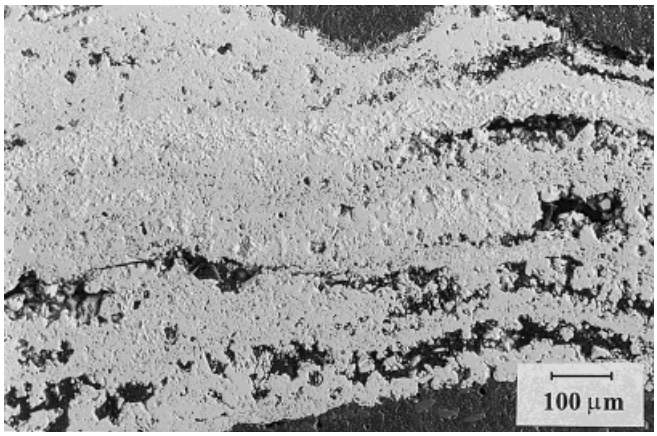

Fig. 15. SEM-image of a metallographic cross section of the oxide scale, formed on St. 35.8. The oxide is very porous and contains layers of the KCl-$ZnCl_2$ melt

Abb. 15. REM-Aufnahme eines metallographischen Querschliffs der Oxidschicht, gebildet auf St. 35.8. Das Oxid ist porös und enthält Schichten der erstarrten KCl-$ZnCl_2$-Schmelze

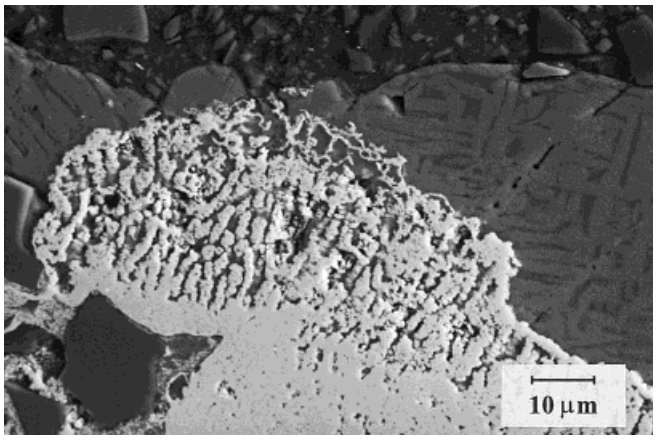

Fig. 17. Precipitates of Fe_2O_3 in the sulfate melt at the scale/SiC phase boundary

Abb. 17. Ausscheidungen von Eisenoxiden in der Sulfatschmelze an der Phasengrenze Oxidschicht/SiC

heavy-metal components such as lead and/or zinc. The chloride melt is within the $ZnCl_2$-KCl system and in some cases also sodium and some lead is found, but no calcium. Considering the heavy-metals more zinc is present than lead and the amount of heavy-metals is much higher in the chloride melt than in the sulfate melt. Especially in the sulfate melts precipitates of iron- and nickel-oxides are found, but no chromia, even in the case of the nickel-based alloy. As corrosion products generally metal-chlorides and -oxides are detected and the oxide contains high amounts of molten salt. In some cases, also sulfide was identified.

3 Thermodynamic considerations

3.1 General remarks

In order to explain the stability of chlorides besides sulfates in deposits, especially with respect to their local distribution within the deposit/scale/metal system and their chemical composition, thermodynamic calculations are carried out and discussed in the following chapter.

At a given partial pressure of oxygen and water the stability of sulfates with respect to chlorides strongly depends on the HCl/SO_2 ratio and also on the temperature of the gas phase and in the deposits on the tubes. Considering the gaseous species O_2, H_2O, HCl and SO_2 to be typical for waste incineration atmospheres, equilibria between sulfates and chlorides are established by the following reactions:

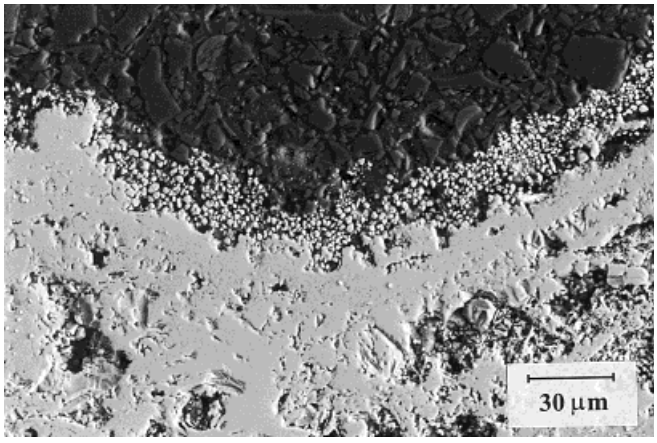

Fig. 16. Precipitates of Fe_2O_3 in the KCl-$ZnCl_2$-melt at the scale/SiC phase boundary

Abb. 16. Ausscheidungen von Fe_2O_3 in der KCl-$ZnCl_2$ Schmelze an der Phasengrenze Metall/SiC Material

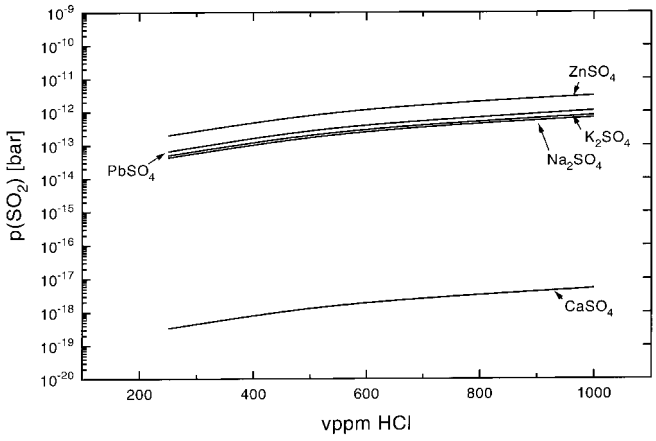

Fig. 18. Sulfate/chloride equilibria as a function of p(HCl) and $p(SO_2)$ for constant $p(H_2O) = 0.03$ bar and constant $p(O_2) = 0.05$ bar at 400 °C

Abb. 18. Sulfat-/Chloridgleichgewichte als Funktion von p(HCl) und $p(SO_2)$ für konstant $p(H_2O) = 0{,}03$ bar und konstant $p(O_2) = 0{,}05$ bar bei 400 °C

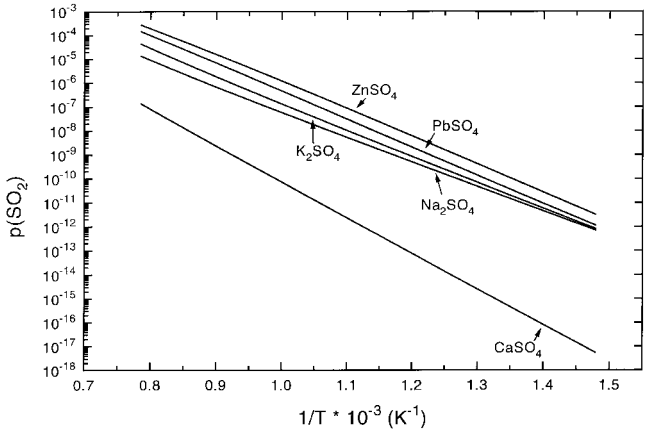

Fig. 19. Sulfate/chloride equilibria as a function of temperature for constant $p(H_2O) = 0.03$ bar, constant $p(O_2) = 0.05$ bar and constant $p(HCl) = 1000$ vppm

Abb. 19. Sulfat-/Chloridgleichgewichte als Funktion der Temperatur für konstant $p(H_2O) = 0{,}03$ bar, konstant $p(O_2) = 0{,}05$ bar und konstant $p(HCl) = 1000$ vppm

$$K_2SO_4 + 2\ HCl = 2\ KCl(s) + SO_2 + 1/2\ O_2 + H_2O \quad (9)$$

$$Na_2SO_4 + 2\ HCl = 2\ NaCl(s) + SO_2 + 1/2\ O_2 + H_2O \quad (10)$$

$$CaSO_4 + 2\ HCl = CaCl_2(s) + SO_2 + 1/2\ O_2 + H_2O \quad (11)$$

$$ZnSO_4 + 2\ HCl = ZnCl_2(g) + SO_2 + 1/2\ O_2 + H_2O \quad (12)$$

$$PbSO_4 + 2\ HCl = PbCl_2(g) + SO_2 + 1/2\ O_2 + H_2O \quad (13)$$

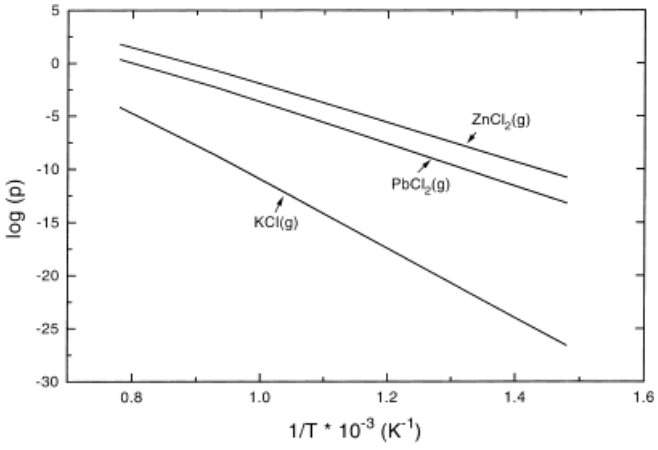

Fig. 20. Partial pressure of volatile $PbCl_2$, $ZnCl_2$ and KCl as a function of temperature for constant $p(H_2O) = 0.03$ bar, constant $p(O_2) = 0.05$ bar, constant $p(HCl) = 1000$ vppm and constant $p(SO_2) = 100$ vppm

Abb. 20. Partialdrücke des flüchtigen $PbCl_2$, $ZnCl_2$ und KCl als Funktion der Temperatur für konstant $p(H_2O) = 0{,}03$ bar, konstant $p(O_2) = 0{,}05$ bar, konstant $p(HCl) = 1000$ vppm und konstant $p(SO_2) = 100$ vppm

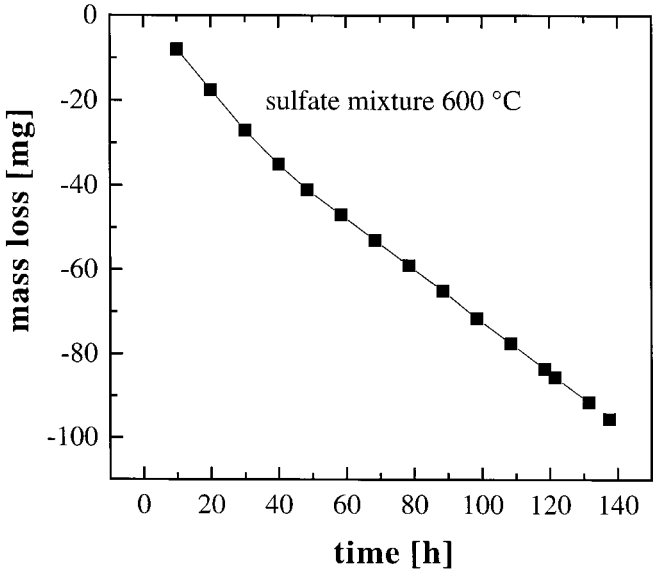

Fig. 21. Mass loss of a $CaSO_4$-K_2SO_4-Na_2SO_4-$PbSO_4$-$ZnSO_4$ salt mixture in He – 5 vol.% O_2 – 1000 vppm HCl at 600 °C due to the formation of $PbCl_2(g)$ and $ZnCl_2(g)$

Abb. 21. Massenabnahme einer $CaSO_4$-K_2SO_4-Na_2SO_4-$PbSO_4$-$ZnSO_4$-Salzmischung in He – 5 vol.% O_2 – 1000 vppm HCl bei 600 °C aufgrund der Bildung von flüchtigem $PbCl_2$ und $ZnCl_2$

In the case of $ZnSO_4$ and $PbSO_4$ volatile chlorides will be formed at temperatures of 400 °C and higher. In Fig. 18 the equilibria (9)–(13) are plotted as a function of p(HCl) and $p(SO_2)$, Fig. 19 shows these equilibria as a function of temperature for an atmosphere containing 1000 vppm HCl, which is a representative concentration in waste incineration plants. All calculations are done for constant $p(H_2O)$ 0.03 bar and constant $p(O_2)$ 0.05 bar.

From these diagrams, the following conclusion are drawn:

- The partial pressure of SO_2 necessary for stabilization of sulfates increases with increasing p(HCl).
- Calcium sulfate is much more stable with resepct to the corresponding chlorides than the sulfates of sodium, potassium, lead and zinc. The heavy-metals form the less stable sulfates, especially $ZnSO_4$ is most easily converted.
- With respect to the sulfates chlorides are more stable at higher temperatures. At a given $p(HCl)/p(SO_2)$ ratio, sulfates become more stable with decreasing temperature.

Considering the atmosphere, containing 1000 vppm hydrogen chloride (Fig. 19) at 1000 °C, calcium sulfate is stable. The equilibrium partial pressure of SO_2 for conversion of the chloride to the sulfate is approx. 0.1 vppm, which is exceeded in most plants (Table 1) and, therefore, $CaSO_4$ is more stable than $CaCl_2$. The alkali-sulfates Na_2SO_4 and especially K_2SO_4 are less stable, the equilibrium partial pressures is in the range of approx. 10–50 vppm SO_2, which is not always reached in waste fired boilers. Hence, NaCl and KCl may be formed at higher temperatures and will be converted to sulfates with decreasing temperatures of the flue gas. The heavy-metal sulfates $PbSO_4$ and $ZnSO_4$ are much easier converted to chlorides, the equilibrium partial pressure of SO_2 necessary for their stability is in the range of approx. 100–500 vppm at 1000 °C, which is rather high for waste incineration plants, and, therefore, gaseous $PbCl_2$ and $ZnCl_2$ are supposed to be stable at higher temperatures and will be converted to sulfates only by cooling down the gas. Considering

the volatile species, Fig. 20 shows the partial pressure of gaseous $ZnCl_2$, $PbCl_2$ and KCl in equilibrium with the corresponding sulfates as a function of temperature for the atmosphere containing 1000 vppm HCl, 100 vppm SO_2, 0.05 bar O_2 and 0.03 bar H_2O. At any temperature fixed partial pressures of volatile species exist in equilibrium, which decrease with decreasing temperature and, compared to KCl(g), are quite high for $ZnCl_2$(g) and $PbCl_2$(g). Cooling down from higher temperatures shifts equilibrium of reaction (12) and (13) to the left and the atmosphere becomes oversaturated with gaseous $ZnCl_2$ and $PbCl_2$, leading to dumping at the condensation temperatures.

In Fig. 21, a thermogravimetric curve is shown of the mass change of the sulfate mixture, used for the exposure experiments in chapter 4 during reaction at 600 °C with a gas atmosphere containing He – 5 vol.% O_2 – 1000 vppm HCl. A significant mass loss is observed, indicating the evaporation of $ZnCl_2$(g) and $PbCl_2$(g), which were found as condensates in the cooler parts of the reaction tube. This experiment clearly shows the reaction of a liquid sulfate mixture to volatile heavy-metal chlorides. It has to be mentioned that the equilibrium state of the gas is quite uncertain due to the fast flowing velocity of the gas stream. As a consequence more alkali-chlorides will survive in the cooler part of the furnace and, therefore, be included in the deposits, whereas the volatile heavy-metal chlorides will dump out of the gas phase when reaching a cooler tube surface.

In conclusion, if equilibrium is established in the gas phase, chlorides formed at high temperatures will be converted to sulfates in the flue gas with decreasing temperature. From this point of view, mostly sulfates should be stable in the deposits, formed in the low temperature regions of the boiler i. e. the superheater section. The equilibrium amount of solid chlorides will be very small, and the most possible phases will be KCl and NaCl rather than $CaCl_2$. This is in good agreement with the occurrence of chloride phases in the deposits described before. In addition, volatile $ZnCl_2$ and $PbCl_2$ are stable in equilibrium with the related sulfates, tending to condensate at lower temperatures. If the gas is in the nonequilibrium state, more chlorides are supposed to be found in the deposits, especially heavy-metal chlorides, KCl and NaCl rather than $CaCl_2$.

Considering the formation of a deposit, the gas is supposed to be in the nonequilibrium state and, therefore, sulfates are stable besides certain amounts of chlorides, stemming from the high temperature region of the boiler ($ZnCl_2$(g), $PbCl_2$(g), KCl(s, g), NaCl(s, g)). As the vapour pressure of sulfates and alkali-chlorides is much lower than for heavy-metal chlorides, they will condense on the fly ash particles at relatively high temperatures within the flowing gas. Striking a cool superheater surface, the heavy-metal chlorides will condense on the tube, including the fly ash particles with the sulfate and chloride condensate. In the presence of heavy-metal chlorides liquid phases are formed, preferentially low melting eutectics, due to the low temperature of the tube surface (see also Table 3). These eutectics are usually formed by chlorides, especially from the KCl-$ZnCl_2$ system, as observed in the deposits described before. Mainly $ZnCl_2$ was found as a heavy-metal compound at the deposit scale interface, because it has the highest vapour pressure, as shown in Fig. 20. As long as the deposit is thin, the amount of heavy-metal chlorides decreases within the gas stream and only sulfates remain with the silica spheres. For this reason, the tube of analysis No. 1 only shows chlorides at the front and not on the left and right hand side, where mainly sulfates were detected. If a deposit has been formed on the tube, a temperature gradient is established throughout the deposit from the hotter part, i.e. the deposit/gas interface, to the cooler part, i.e. the scale/deposit interface. As shown by analysis of deposits, sulfates are found at the deposit/gas interface whereas the chlorides are found at the deposit/scale interface. The occurrence of a sulfate melt, at the deposit/gas phase boundary shows that nearly equilibrium is established between the outer part of the deposit and the gas phase, in contrast to the inner part which is far from equilibrium with the gas phase, indicated by the high amount of chlorides. The sulfate melt will inhibit the diffusion of gas species into the deposit and, therefore, the chloride melt at the tube surface will remain stable. In addition, the sulfates in contact with the gas will establish $p(SO_2)$ in the deposits by the reaction (9)–(13). As mainly $CaSO_4$ is present, $p(SO_2)$ will be too low to convert heavy-metal chlorides and also KCl to a sulfate. With time, the condensation of the heavy-metal chlorides will move towards the plant, according to the increasing temperature of the deposit surface. Removal of thick deposits from the tubes and water walls will result in a new accelerated attack by the condensing chloride and should be avoided in order to prevent condensation. In the cases where no chlor-

Table 8. Salt mixtures (wt.%) used in the exposure tests
Tabelle 8. Zusammensetzung der Salzmischungen (Gew.%) für die Auslagerungsexperimente

mixture	$CaSO_4$	K_2SO_4	Na_2SO_4	$PbSO_4$	$ZnSO_4$
1	50	29	21	–	–
2	39	22.5	16	22.5	–
3	46	27	19	–	8
4	36	21	15	21	7

Table 7. Composition (wt.%) of the alloy used in the thermogravimetric experiments and exposure tests
Tabelle 7. Chemische Zusammensetzung (Gew.%) der in thermogravimetrischen und Auslagerungsexperimenten verwandten Legierungen

	Fe	Cr	Ni	Si	others
10 CrMo 9 10	bal.	2.21	–	–	Mo: 0.91
X 20 CrMoV 12 1	bal.	10/12.5	–	–	V: 0.25/0.35
X 5 NiCrCeNb 32 27	bal.	27.35	31.45	0.21	Nb: 0.83; Ce: 0.09
Alloy 602 CA	9.65	25.3	bal.	–	Al: 2.13
Inconel 625	4.65	22.2	bal.	0.09	Mo: 9.2; Nb: 3.5
Alloy 45 TM	22.65	27.40	bal.	2.66	Mn: 0.36

ides are present, the sulfate melt will attack the tube, as indicated by oxide precipitates in the sulfate melt.

This model, based on thermodynamic calculations explains quite clearly the occurrence of low melting chloride and sulfate melts in the deposits, especially with reference to their local distribution. It also explains the chemistry of the salts, especially the formation of $ZnCl_2$-rich chlorides and the instability of $CaCl_2$ in the ashes. Once formed, the chloride and also the sulfate melts will attack material very severely, as described in the next chapters.

4 Experimental studies

4.1 Experimental setup and materials

In the case of molten chlorides the laboratory studies were carried out using thermogravimetric experiments or in the case of experiments beneath sulfate deposits with exposures. The thermogravimetric experiments were carried out in a horizontal microbalance, connected to a gas mixing equipment. This setup was described in detail in a previous publication [10]. The thermogravimetric experiments were carried out in a He – 5 vol.% O_2 atmosphere with a water content less than 10^{-4} bar at temperatures ranging from 300–600 °C. The salts used, were $PbCl_2$, $ZnCl_2$ and a 50 wt.% $ZnCl_2$ – 50 wt.% KCl mixture. The testing gas was established by mixing the commercial bottled gases helium and oxygen which were dried by passing through columns filled with P_2O_5. The salt was deposited after 24 h of preoxidation on top of the oxide scale, the amount of salt was 15 mg/cm^2. The materials used were 10 CrMo 9 10, X5 NiCrCeNb 32 27 (AC 66) and Inconel 625, their compositions are given in Table 7. Before starting the experiments, the samples were ground with 1000 grid SiC-paper, measured and cleaned in acetone in an ultrasonic bath.

The furnace for the exposures was connected in the same way, however, the N_2 – 5 vol.% O_2 mixture was supplied as a premixed commercial gas. The gas was also dried by passing through columns filled with P_2O_5 before entering the furnace. According to the large temperature constant zone, it was possible to test 24 samples at the same time. The exposure experiments were carried out at 600 °C, using different sulfate mixtures (shown in Table 8) and also different metallic materials, listed in Table 7. The samples were preoxidized in N_2 – 5 vol.% O_2 for 5 h at 600 °C and embedded in approx. 1.5 g of the salt mixture afterwards. The extent of corrosion was determined by measuring the mass loss after 360 h of reaction after removal of the corrosion products by chemical etching in a $KMnO_4$-NaOH-solution at 80 °C. The samples were prepared by grinding with 600 grid SiC-paper, measuring and weighing before the experiments.

Investigation of the corroded samples were carried out by X-ray diffraction (XRD) in order to analyse the phases formed during corrosion. In addition, scanning electron microscopy (SEM) and energy dispersive X-ray analysis (EDX) was used to study the morphology and the chemical composition of the corrosion products. The investigations were carried out on corroded surfaces as well as on metallographic cross sections.

4.2 Thermogravimetric experiments with $PbCl_2$ and $ZnCl_2$

4.2.1 $PbCl_2$

Fig. 22 shows the mass gain of the 10 CrMo 9 10 after deposition of 15 mg/cm^2 of $PbCl_2$ on to the scale, formed during 24 h of preoxidation in He – 5 vol.% O_2. The corrosion is markedly enhanced at 500 and also at 600 °C compared to normal oxidation rate. The $PbCl_2$ deposit is molten at reaction temperature and, therefore, the corrosive attack occurs by the chloride melt. Investigation of the scale after the experiments show elongated Fe_2O_3 crystals with smooth surfaces, growing towards the gas atmosphere (Fig. 23). Looking at metallographic cross section in Fig. 24, a badly adherent and cracked

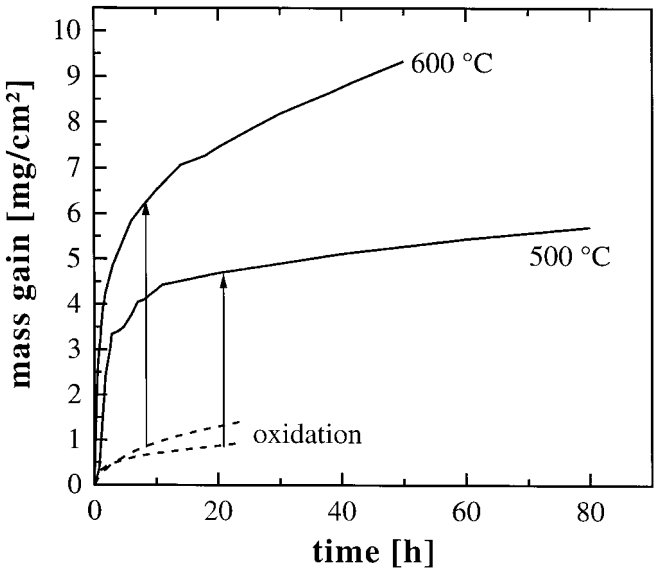

Fig. 22. Mass gain of 10 CrMo 9 10 after deposition of 15 mg/cm^2 $PbCl_2$ on top of the oxide scale of the preoxidized sample in He – 5 vol.% O_2. The corrosion is markedly enhanced at 500 and 600 °C compared to oxidation without the salt

Abb. 22. Massenzunahme von 10 CrMo 9 10 nach Zugabe von 15 mg/cm^2 $PbCl_2$ auf die Oberfläche der Oxidschicht der voroxidierten Probe in He – 5 vol.% O_2. Die Korrosion ist bei 500 und 600 °C stark beschleunigt

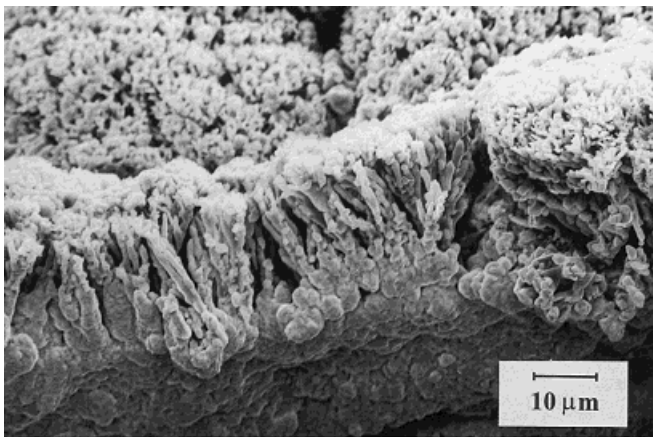

Fig. 23. Elongated iron oxide crystals, growing towards the gas atmosphere

Abb. 23. Längliche Eisenoxidkristalle, in Richtung Gasatmosphäre wachsend

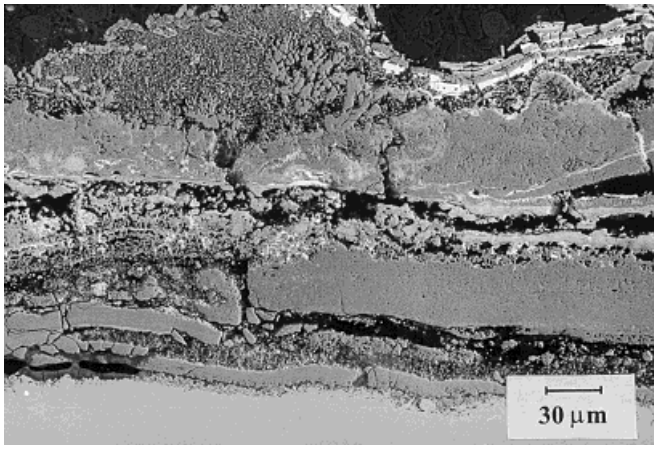

Fig. 24. SEM-image of a metallographic cross section of 10 CrMo 9 10 after corrosion in contact with $PbCl_2$ in He – 5 vol.% O_2 at 500 °C. Especially at the scale/gas interface Fe_2O_3-particles are precipitated

Abb. 24. REM-Aufnahme eines metallographischen Querschliffs von 10 CrMo 9 10 nach Korrosion in Kontakt mit $PbCl_2$ in He – 5 vol.% O_2 bei 500 °C. Besonders an der Phasengrenze Schicht/Gas haben sich Fe_2O_3-Teilchen ausgeschieden

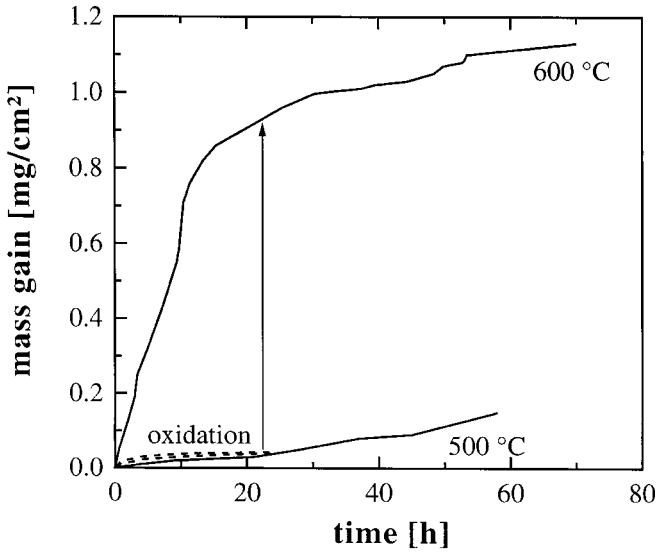

Fig. 25. Mass gain of AC 66 after deposition of 15 mg/cm^2 $PbCl_2$ on top of the oxide scale of the preoxidized sample in He – 5 vol.% O_2. The corrosion is enhanced at 500 and 600 °C compared to oxidation without the salt, however, it is much less as observed on 10 CrMo 9 10

Abb. 25. Massenzunahme von AC 66 nach Aufbringen von 15 mg/cm^2 $PbCl_2$ auf die Oberfläche der Oxidschicht der voroxidierten Probe in He – 5 vol.% O_2. Im Vergleich zur Massenzunahme durch Oxidation ohne Salz ist die Korrosion bei 500 und 600 °C stark beschleunigt, jedoch geringer als an 10 CrMo 9 10 beobachtet

scale was found. At the scale/gas interface Fe_2O_3 particles are visible, precipitating out of the melt. All over the scale small amounts of Pb are detected, however, no lead containing phase was found with XRD. At the metal/scale interface, small amounts of chlorine together with iron, probably $FeCl_2$, are identified.

According to the precipitation of Fe_2O_3 at the scale/gas interface, a fluxing mechanism is suggested. The oxide scale is dissolved in the $PbCl_2$ melt at the melt/scale phase boundary at low oxygen partial pressures under formation of soluble $FeCl_x$:

$$Fe_2O_3 + 6\ Cl^-_{(PbCl2)} = 2\ FeCl_3\ (diss.) + 3\ O^{2-}_{(PbCl2)} \qquad (14)$$

The dissolved $FeCl_x$ diffuses along the concentration gradient through the melt film to the melt/gas interface, where a higher $p(O_2)$ is established and, therefore, Fe_2O_3 is formed:

$$2\ FeCl_3\ (diss.) + 3/2\ O_2 = Fe_2O_3(s) + 3\ Cl_2 \qquad (15)$$

The Fe_2O_3 precipitates at the melt/gas interface, releasing chlorine gas, which leads to the formation of additional $FeCl_x$. The overall mass gain of the reactions (13) and (14) is zero, however, an unprotective scale is formed and the oxidation of the metal is significantly accelerated.

The results of experiments on AC 66 with $PbCl_2$ deposits under the same conditions are shown in Fig. 25. In comparison with the normal oxidation rate, the corrosion is also enhanced, but much less than in the case of the low alloy 10 CrMo 9 10 steel. As corrosion products, mainly voluminous Fe_2O_3 and $PbCrO_4$ are detected in top of the sample. The insoluble solid $PbCrO_4$ is formed by reaction:

$$2\ PbCl_2(l) + Cr_2O_3 + 5/2\ O_2 = 2\ PbCrO_4 + 2\ Cl_2 \qquad (16)$$

Investigation of metallographic cross sections exhibit a compact scale on top of the alloy, as shown in Fig. 26. Underneath the scale, a zone of significant internal attack is visible, the corrosion product consists mainly of spinel $FeCr_2O_4$. In addition, also small amounts of chlorine are detectable. The remaining metal (white phase) is nickel, enriched with some niobium. In contrast to the low alloy steel, no fluxing of the scale takes place in this case, as $PbCrO_4$ is an insoluble corrosion product. The internal oxide growth is due to the attack of carbide precipitates by chlorine, formed by reaction (16). The main corrosion mechanism is active oxidation, indicated by the formation of voluminous Fe_2O_3 on top of the scale and significant internal attack under formation of a metal-chloride-spinel mixture.

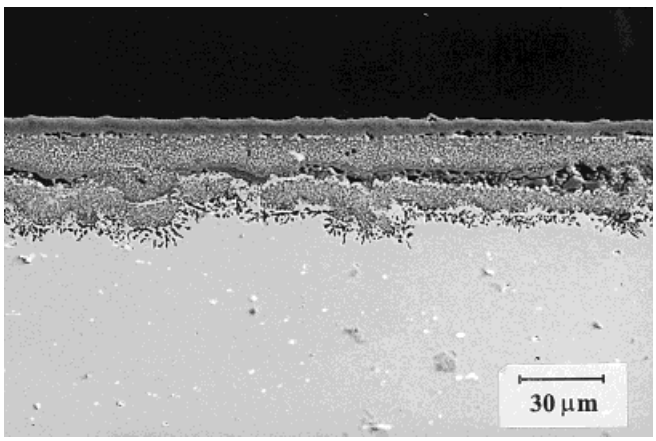

Fig. 26. SEM-image of a metallographic cross section of AC 66 after corrosion in contact with $PbCl_2$ in He – 5 vol.% O_2 at 500 °C. Underneath an outer compact scale, significant inward growth of oxide into the metal is observed

Abb. 26. REM-Aufnahme eines metallographischen Querschliffs von AC 66 nach Korrosion in Kontakt mit $PbCl_2$ in He – 5 vol.% O_2 bei 500 °C. Unter einer kompakten äusseren Schicht ist ein Einwachsen von Oxid in die metallische Matrix zu beobachten

4.2.2 Influence of $ZnCl_2$

The influence of $ZnCl_2$ on the corrosion on the 10 CrMo 9 10 steel is shown in Fig. 27. At 500 °C no significant corrosion takes place, whereas at 600 °C the corrosion rate is markedly enhanced compared to the normal oxidation rate.

Investigations of the sample, reacted at 500 °C show an oxide scale, consisting of mainly Fe_3O_4 and $ZnFe_2O_4$. Obviously, the Fe_2O_3 formed during preoxidation is consumed by reaction with the salt melt. In metallographic cross sections, a relatively dense scale was found with SEM, exhibiting a thin layer of (Zn,Fe)O on top. At the metal/scale interface, small amounts of chlorine in combination with iron are detected with EDX measurements. In addition, EPMA linescans were carried out, indicating an inward diffusion of zinc into the scale, as shown in Fig. 28. The amount of zinc on top of the scale was measured to be about 32 at.%, the amount of iron about 17 at.% and oxygen was measured to be close to 50 at.%. This indicates a MO-oxide, with a stochiometric composition close to (Zn,Fe)O. This oxide forms the outer scale up to approx. 4 µm thickness. Within these 4 microns, the iron content increases whereas the zinc content decreases with increasing distance from the scale/gas phase boundary, however, the total sum of cations is nearly 50 at.%. According to these results, ZnO must have been formed on the surface of the scale, incoporating iron ions and consuming Fe_2O_3, formed during preoxidation. As the oxygen content is very low at the melt/scale phase boundary, Fe_2O_3 can be reduced to form Fe_3O_4 according to:

$$ZnCl_2(l) + 2\ Fe_2O_3 = (Zn,\ Fe)O + Fe_3O_4 + Cl_2 + 1/2\ O_2 \quad (17)$$

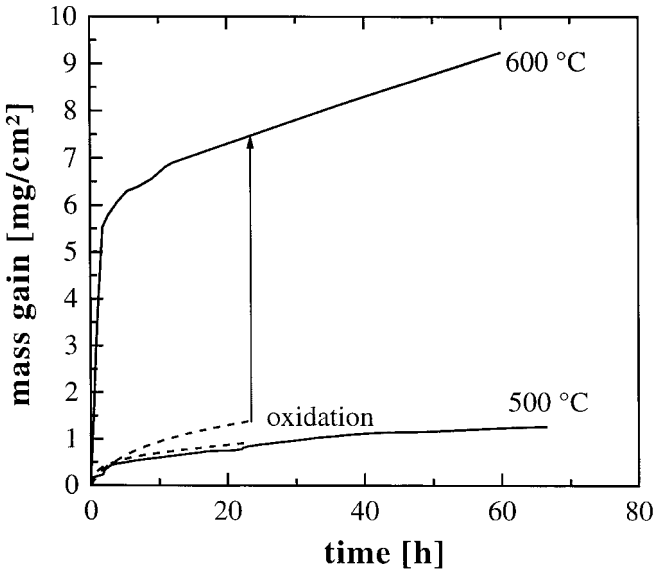

Fig. 27. Mass gain of 10 CrMo 9 10 after deposition of 15 mg/cm^2 $ZnCl_2$ on top of the oxide scale of the preoxidized sample in He – 5 vol.% O_2. The corrosion is markedly enhanced at 600 °C compared to oxidation without the salt. At 500 °C, no significant attack is observed

Abb. 27. Massenzunahme von 10 CrMo 9 19 nach Zugabe von 15 mg/cm^2 $ZnCl_2$ auf die Oberfläche der Oxidschicht der voroxidierten Probe in He – 5 vol.% O_2. Im Vergleich zur Oxidation ohne Salz ist die Korrosion bei 600 °C stark beschleunigt. Bei 500 °C ist kein signifikanter Abgriff zu beobachten

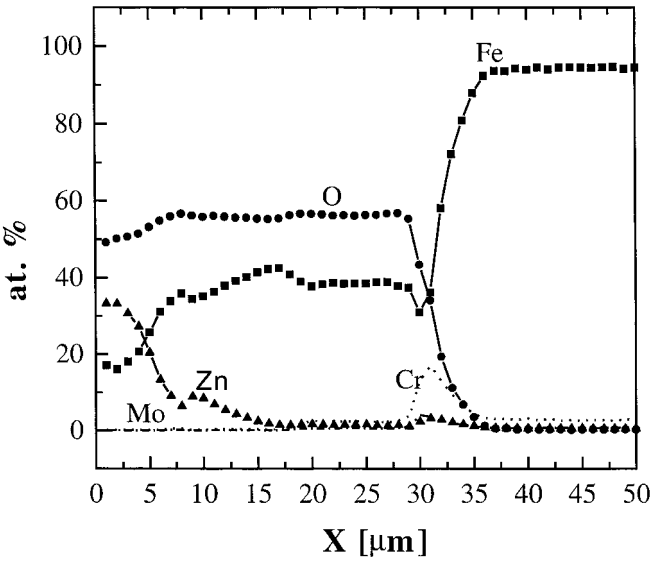

Fig. 28. EPMA-linescan through the oxide scale formed on 10 CrMo 9 10 after reaction with $ZnCl_2$ in He – 5 vol.% O_2 at 500 °C. The linescan shows quite clearly the inward diffusion of zinc into the scale

Abb. 28. ESMA-Linescan durch die Oxidschicht von 10 CrMo 9 10 nach Reaktion mit $ZnCl_2$ in He – 5 vol.% O_2 bei 500 °C. Der Linescan zeigt deutlich die Einwärtsdiffusion von Zink in die Schicht

As there are only small amounts of $FeCl_2$ detected at the metal/scale interface, most of the chlorine is supposed to get lost into the gas atmosphere.

Moving into the scale, the oxygen content increases approaching a final value of about 58 at.% after approx. 7.5 µm, which is close to the spinel composition AB_2O_4. The total sum of cations is 42.857 at.% theoretically, which is closely reached by the sum of iron and zinc in the spinel measured here. Obviously iron is replaced by zinc in the scale. Considering the magnetite structure, the formula can be written as $(Fe^{2+}, Zn^{2+})\ Fe_2^{3+}\ O_4$ with decreasing zinc and increasing iron content moving towards the metal/scale interface. After approx. 17 µm, the spinel has the stochiometric Fe_3O_4 composition. The area between 4 and 7.5 µm is characterized by a transition zone between the MO oxide

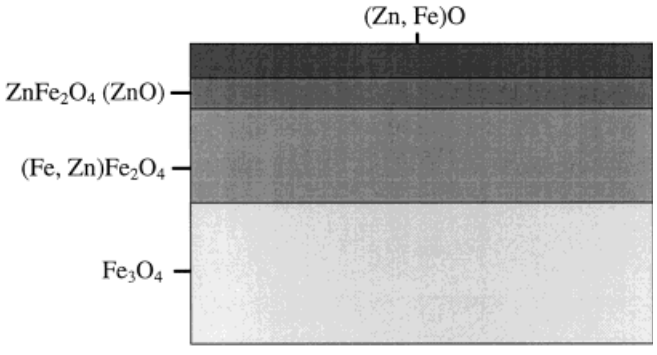

Fig. 29. Schematic plot of the oxide layers, formed on 10 CrMo 9 10 after reaction with $ZnCl_2$ in He – 5 vol.% O_2 at 500 °C

Abb. 29. Schematische Darstellung der Oxidschichten, gebildet auf 10 CrMo 9 10 nach Reaktion mit $ZnCl_2$ in He – 5 vol.% O_2 bei 500 °C

and the spinel, probably caused by an excess of dissolved ZnO in the $ZnFe_2O_4$. In Fig. 29, a schematic plot of the scale composition is shown. In contrast to the experiments with $PbCl_2$, the spinel which forms under these conditions is insoluble in the $ZnCl_2$-melt and, therefore, no fluxing of the scale takes place. The Fe_2O_3 is completely consumed by reaction (16) and the scale consists mainly of spinel (Fe, Zn)Fe_2O_4 and Fe_3O_4. According to the mass gain observed, the growth rate of the scale is comparable to the growth kinetics of the Fe_2O_3/Fe_3O_4 oxide layer, formed during oxidation in the same gas mixture.

Investigations of the scale, formed at 600 °C indicates no zinc-spinel formation and a much thicker scale. In this case, the EPMA analysis indicates only small concentrations of zinc (up to 1 at.%) in the outer parts of the scale and dissolved zinc all over the magnetic phase. In contrast to the oxide, formed at 500 °C, the scale consists of an outer layer of haemetite (Fe_2O_3) and an inner layer of magnetite with some dissolved zinc (Fe_3O_4). At the metal/scale interface, also small amounts of $FeCl_2$ are detected. It has to be considered that evaporation of $ZnCl_2$ takes place during the experiments and, therefore, the reaction time between the melt and the scale will be much shorter at 600 °C than at 500 °C, which will lead to the different phases, formed during corrosion. The magnetite scale is much thicker and the kinetics of corrosion much faster than in the case of oxidation without the salt. For this reason, the growth of the magnetite scale seems to be somewhat accelerated, probably by incooperating small amounts of ZnO into the magnetite structure. It is well known from other spinels like $CoFe_2O_4$ that incooperation of divalent oxides like CoO or MgO will increase the tracer diffusion coefficient for the cations in these compounds [16]. Hence, it is likely that excess of ZnO in the Fe_3O_4 phase will lead to accelerated diffusion of iron in the scale accompanied by a faster scale growth.

Fig. 30 shows the effect of $ZnCl_2$ on the corrosion of the high alloy steel AC 66. The corrosion is slightly enhanced compared to the normal oxidation rate and comparable to that, observed beneath the $PbCl_2$ melt. The mass gain is much higher at 600 °C than at 500 °C. At both temperatures, mainly Cr_2O_3, Fe_2O_3 and ZnO were formed and, in some cases, also a zinc-rich spinel (Fe, Zn)Cr_2O_4 was identified by XRD containing chromium and iron but no nickel. The ZnO on top of the sample is formed by reaction of the $ZnCl_2$ melt with the gas phase, releasing chlorine:

$$ZnCl_2 + 1/2\ O_2 = ZnO + Cl_2 \qquad (18)$$

in a further reaction, spinel is formed by reaction of ZnO with the chromia scale:

$$ZnO + Cr_2O_3 = ZnCr_2O_4 \qquad (19)$$

As already observed in the experiments with $PbCl_2$, the alloy shows significant internal attack after reaction with $ZnCl_2$. Besides oxygen, also chlorine was detected by EDX, obviously chlorides are present as corrosion products. The remaining metal is enriched in nickel. The chlorine, formed by reaction (18) leads to the formation of metal chlorides at the scale/metal interface, causing active oxidation and, therefore, severe corrosion. This is also indicated by the formation of Fe_2O_3 on top of the scale. Hence, also in this case, insoluble corrosion products, like ZnO and $ZnCr_2O_4$ have formed in contact with the $ZnCl_2$ melt and, therefore, no fluxing of the scale takes place.

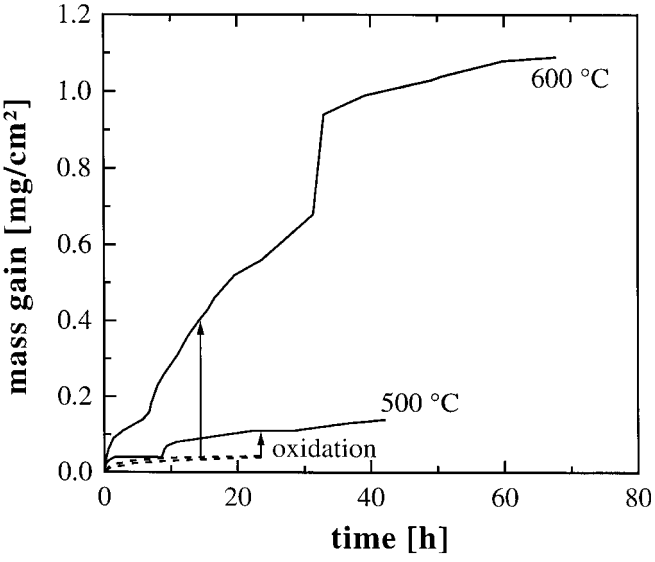

Fig. 30. Mass gain of AC 66 after deposition of 15 mg/cm^2 $ZnCl_2$ on top of the oxide scale of the preoxidized sample in He – 5 vol.% O_2. The corrosion is slightly enhanced at both temperatures and much less compared to 10 CrMo 9 10

Abb. 30. Massenzunahme von AC 66 nach Aufbringen von 15 mg/cm^2 $ZnCl_2$ auf die Oberfläche der Oxidschicht der voroxidierten Probe in He – 5 vol.% O_2. Die Korrosion ist bei beiden Temperaturen geringfügig erhöht und deutlich geringer als im Vergleich mit 10 CrMo 9 10

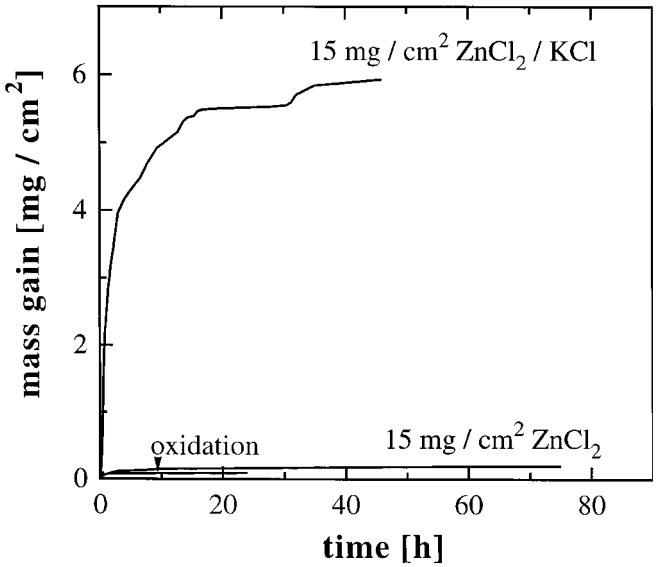

Fig. 31. Mass gain of 10 CrMo 9 10 after deposition of 15 mg/cm^2 $ZnCl_2$-KCl mixture on top of the oxide scale of the preoxidized sample in He – 5 vol.% O_2. The corrosion is significantly enhanced at 400 °C compared to oxidation without the salt and in contact with 15 mg/cm^2 $ZnCl_2$

Abb. 31. Massenzunahme von 10 CrMo 9 10 nach Zugabe von 15 mg/cm^2 $ZnCl_2$-KCl auf die Oberfläche der Oxidschicht der voroxidierten Probe in He – 5 vol.% O_2. Die Korrosion ist bei 400 °C stark erhöht im Vergleich zur Oxidation ohne Salz und mit 15 mg/cm^2 $ZnCl_2$

From the experiments at 400 °C with $PbCl_2$, $ZnCl_2$ and also KCl no significant corrosion occurs of low and high alloy steels in an oxidizing gas mixture.

4.3 Thermogravimetric experiments with a $ZnCl_2$-KCl mixture

Considering the results in chapter 2, molten chloride phases, consisting of $ZnCl_2$ and KCl as the major components were identified in deposits from waste fired boilers. Hence, after studying the effect of the molten chlorides $PbCl_2$ and $ZnCl_2$, studies about corrosion mechanisms in contact with molten chloride mixtures are very important, especially at the relatively low temperatures on the surface of the superheater tubes and water walls within the boiler. In order to study the effect of a molten chloride mixture, experiments were carried out with a 50 wt.% $ZnCl_2$ – 50 wt.% KCl salt mixture in the temperature range of 300–400 °C in a He – 5 vol.% O_2 atmosphere.

Fig. 31 shows the mass gain due to corrosion of the 10 CrMo 9 10 alloy in contact with 15 mg/cm^2 of the 50 wt.% KCl – 50 wt.% $ZnCl_2$ mixture. In comparison with the same alloy in contact with 15 mg/cm^2 $ZnCl_2$, the mass gain is enhanced significantly. The salt is molten at reaction temperature so that the attack occurs by the chloride melt. In Fig. 32, a SEM-image of a metallographic cross section after the attack is shown. A thick oxide scale has formed on the alloy, exhibiting different morphologies. On top of the scale, at the former melt/scale phase boundary, there is a very fine grained corrosion product, containing mainly iron and also zinc. Underneath this zone a dense scale of Fe_2O_3 has formed. The outer part of the scale consists of Fe_2O_3 and no zinc was found all over the oxide by EDX-measurements. The inner part, separated by a small gap, is a Fe_3O_4

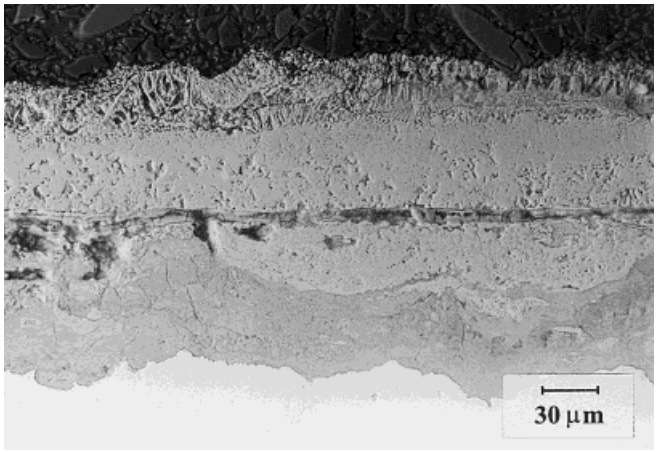

Fig. 32. SEM-image of a metallographic cross section of 10 CrMo 9 10 after corrosion in contact with a $ZnCl_2$-KCl mixture in He – 5 vol.% O_2 at 400 °C. The scale exhibits different morphologies i.e. a fine grained zinc-containing corrosion product at the melt/scale interface, a thick oxide underneath and a dark phase in contact with the metal containing high amounts of potassium

Abb. 32. REM-Abbildung eines metallographischen Querschliffs von 10 CrMo 9 10 nach Korrosion in Kontakt mit einer $ZnCl_2$-KCl Mischung in He – 5 vol.% O_2 bei 400 °C. Die Schicht zeigt unterschiedliche Morphologien, d.h. ein feinteiliges, zinkhaltiges Korrosionsprodukt an der Phasengrenze Schmelze/Schicht, eine dicke Oxidschicht darunter sowie eine dunkle Phase in Kontakt mit dem Metall mit hohen Gehalten an Kalium

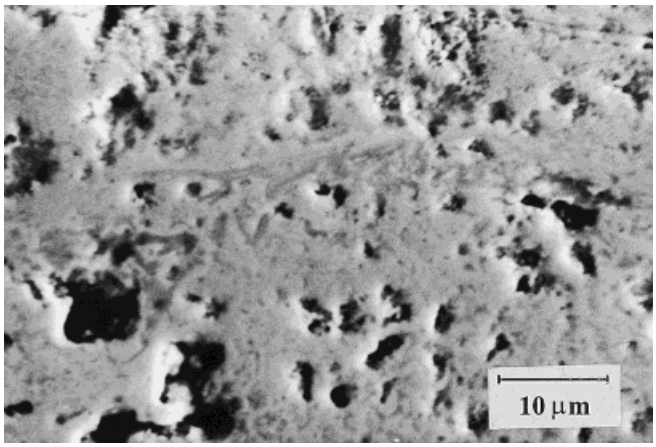

Fig. 33. Band like inclusion in the oxide scale of 10 CrMo 9 10 formed during corrosion in contact with a $ZnCl_2$-KCl mixture in He – 5 vol.% O_2 at 400 °C. In this inclusion chromium, potassium, zinc and chlorine are enriched

Abb. 33. Bandförmige Einschlüsse in der Oxidschicht von 10 CrMo 9 10 gebildet während der Korrosion in Kontakt mit der $ZnCl_2$-KCl-Mischung in He – 5 vol.% O_2 bei 400 °C. In diesen Einschlüssen sind Chrom, Zink und Chlor angereichert

phase with significant amounts of dissolved chromia. This part of the oxide exhibits band like inclusions (Fig. 33), which are enriched in chromium, potassium, zinc and some chlorine. This was also observed in oxide scales from samples of waste incinerator plants. Underneath these iron oxides, a dark phase has formed, mainly containing potassium, iron and oxygen but no chlorine and less chromium than the oxide above. At the metal/scale interface, chlorine was detected in combination with iron, obviously $FeCl_2$.

The results of the experiments show that the $ZnCl_2$-KCl mixture is an extreme corrosive agent and that the addition of $ZnCl_2$ in combination with KCl does not lead to the formation of protective scales of $ZnFe_2O_4$, as in the case of pure $ZnCl_2$ at 500 °C. The occurrence of the fine grained zinc-rich iron oxide at the scale/gas interphase indicates a fluxing mechanism, as observed beneath molten $PbCl_2$ deposits. The iron-oxide scale is dissolved in the melt at low oxygen activities at the melt/oxide interface as $FeCl_3$ by reaction equation (20):

$$Fe_2O_3 + 6\ Cl^-_{(ZnCl2)} = 2\ FeCl_3\ (diss.) + 3\ O^{2-}_{(ZnCl2)} \qquad (20)$$

In contact with the gas phase, precipitation of the dissolved oxide takes place as a zinc-containing phase:

$$2\ FeCl_3\ (diss.) + Zn^{2+}_{(ZnCl2)} + O^{2-}_{(ZnCl2)} + 3/2\ O_2 = ZnFe_2O_4(s) + 3\ Cl_2 \qquad (21)$$

In contrast to experiments beneath pure $ZnCl_2$, the precipitates are forming a non protective corrosion scale. The reaction eqn. (21) leads to a consumption of Zn^{2+} within the melt and, therefore, an enrichment of the KCl component occurs. If the chlorine, liberated by reaction eqn. (21) is dissolved in the melt, $FeCl_3$ and/or $FeCl_2$ are able to form again and the melt is enriched in KCl and iron-chloride with time. The dissolution of iron chloride in the melt decreases the melting point of the salt and, therefore, the salt remains in the molten state, even if Zn^{2+} is consumed by the formation of $ZnFe_2O_4$ (T_m (KCl-$FeCl_2$) = 355 °C). According to the chemistry of the dark

phase underneath the oxide, a Fe-K-O compound has formed, which unfortunately could not be identified by XRD. It is well known from work by *Reese* and *Grabke* [8, 9] that KCl reacts with Fe_2O_3 to form K_2 Fe_2O_4, releasing chlorine gas. It is likely that this compound has also been formed by reaction of the KCl compound in the melt with the Fe-oxide scale or with the alloy itself, however, the occurrence of high oxygen concentrations at the metal/scale interface is rather unusual. As the chromium content of this phase is much lower than those of the oxide scale and, further more, the phase has formed at the metal/scale interface, a reaction of the chloride melt with the alloy is possible after penetration of the KCl enriched salt through cracks and pores of the oxide scale:

$$2\ KCl(1) + 2\ Fe + 2\ O_2 = K_2Fe_2O_4 + Cl_2 \qquad (22)$$

It is important to note that especially K-rich compounds are often observed under oxide scales in samples, reacted in waste incineration plants or as dense layers in oxide scales. A reason for this will be the high viscosity of the K-melt, which leads to a good wetting behaviour and, therefore, penetrates through the oxide scale to the metal scale interface.

In addition, the effect of temperature is shown in Fig. 34. Compared to 400 °C, the initial corrosion rate is less, but still enhanced at 300 and 350 °C. The kinetics of the corrosion process differs significantly, at 400 °C the mass gain decreases after approx. 20 h to normal oxidation rate due to consumption of the salt whereas at 300 °C and 350 °C no retardation was observed even after 100 h. However, the total mass gain will be the same or even more after several hundreds of hours, as already observed in the experiment at 350 °C after 50 h. Investigations of the sample reacted at 300 °C have shown yellow-coloured K-rich zinc- and chlorine-containing crystals within a solidified melt. Obviously, a solid compound has formed, probably K_2ZnCl_4, which was also found as yellow crystals on oxide scales of samples, reacted in waste incineration plants. The morphology of the scale, formed at 300 °C was the same as at 400 °C, i.e. precipitates of zinc-rich oxides at the scale/gas interface, a dense iron-oxide (Fe_2O_3) underneath and a dark phase in contact with the metal. However, in contrast to the scale formed at 400 °C, no potassium and no oxygen was found in the dark phase. It mainly consists of $FeCl_2$, rather than $K_2Fe_2O_4$. This is in good agreement with the model, describing the corrosion process at 400 °C. In this case, the formation of a KCl-$FeCl_2$ eutectic (T_m(KCl-$FeCl_2$) = 355 °C) is not possible and, therefore, KCl is not able to penetrate the scale in liquid form and reacting with the metal.

Fig. 35 shows results of experiments with Inconel 625 in contact with the same amount of salt at 400 °C under the same gas atmosphere. In contrast to the mass gain of the low alloy steels 10 CrMo 9 10, in the first few hours of the experiment the nickel-based alloy shows less corrosion which, however, accelerates very fast afterwards and reaches the same value as for the low alloy steel. The corrosion scale, formed on Inconel 625 is shown in Fig. 36. All over the scale, nickel was detected in combination with chromium and molybdenum. Especially on top, at the scale/gas interface molybdenum was enriched in band like inclusions in the scale. The composition of the scale is quite heterogeneous, Cr-rich areas (dark phase) and Ni-rich areas are distributed all over the oxide. In addition, potassium and zinc are present in the entire scale. These results confirms the observation that Inconel 625 often failed at temperatures from 400 °C in waste incineration plants.

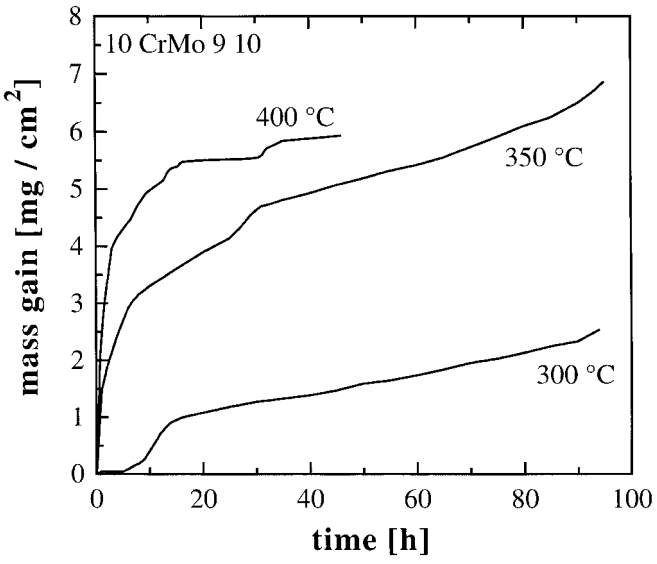

Fig. 34. Temperature dependence of the corrosion rate of 10 CrMo 9 10 beneath the $ZnCl_2$-KCl mixture in He – 5 vol.% O_2. At lower temperatures, the corrosion rate in the beginning of the experiment is less compared to 400 °C. However, the total mass gain can be much higher

Abb. 34. Temperaturabhängigkeit der Korrosionsrate von 10 CrMo 9 10 in Kontakt mit der $ZnCl_2$-KCl Mischung in He – 5 vol.% O_2. Bei niedrigeren Temperaturen wird, im Vergleich zu Experimenten bei 400 °C, anfänglich eine geringere Korrosionsrate beobachtet. Die gesamte Massenzunahme kann jedoch durchaus höher sein

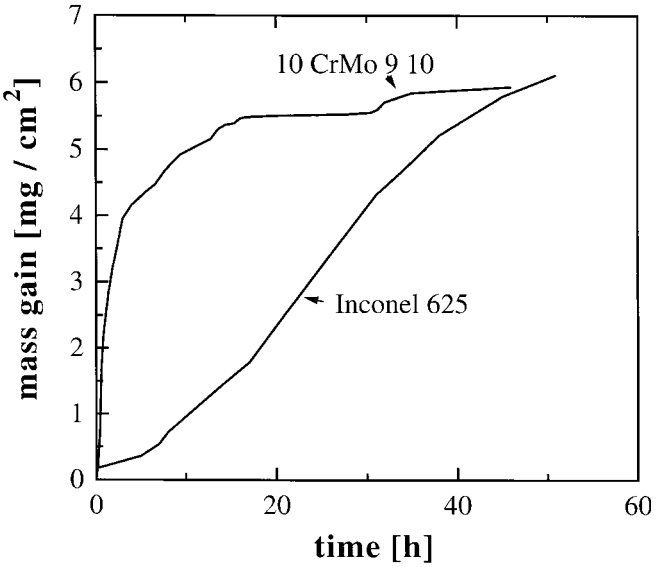

Fig. 35. Mass gain of Inconel 625 in comparison with 10 CrMo 9 10 beneath the $ZnCl_2$-KCl mixture in He – 5 vol.% O_2 at 400 °C. The initial corrosion rate is much less than in the case of 10 CrMo 9 10, however, the total mass gain is the same after 45 h of exposure

Abb. 35. Massenzunahme von Inconel 625 im Vergleich mit 10 CrMo 9 10 in Kontakt mit der $ZnCl_2$-KCl Mischung in He – 5 vol.% O_2 bei 400 °C. Die anfängliche Korrosionsrate ist geringer als bei 10 CrMo 9 10, jedoch ist die absolute Massenzunahme nach 45 h nahezu gleich

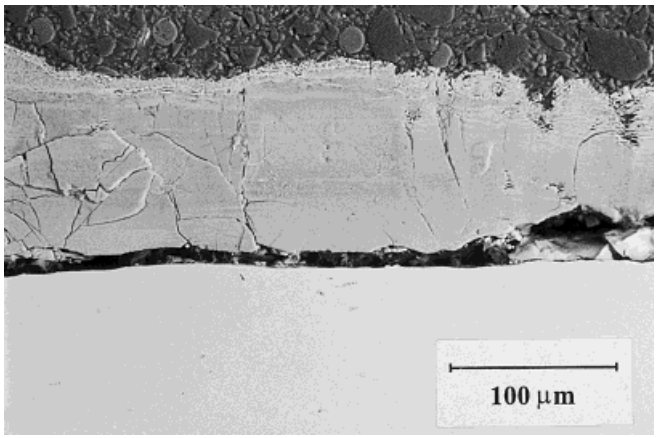

Fig. 36. Corrosion scale on Inconel 625 formed beneath the $ZnCl_2$-KCl mixture in He – 5 vol.% O_2 at 400 °C. The scale has a heterogeneous morphology with bright- and dark-grey coloured areas

Abb. 36. Korrosionsschicht auf Inconel 625, gebildet in Kontakt mit der $ZnCl_2$-KCl Mischung in He – 5 vol.% O_2 bei 400 °C. Die Morphologie der Schicht ist heterogen, man erkennt hell- und dunkelgrau gefärbte Bereiche

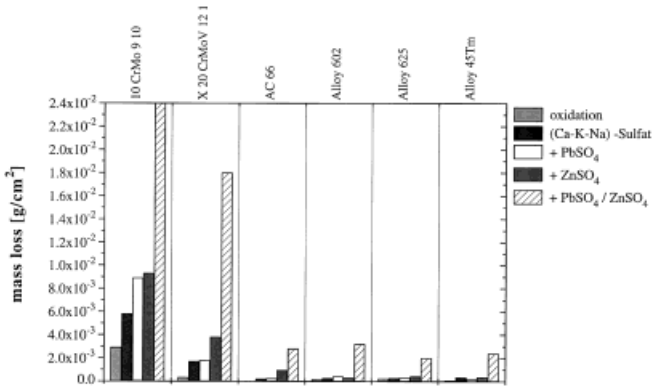

Fig. 37. Mass loss of steels and nickel-based alloys beneath sulfate mixtures in N_2 – 5 vol.% O_2 at 600 °C. The highest mass loss is observed beneath the $PbSO_4$-$ZnSO_4$ containing deposit, which is molten at 600 °C

Abb. 37. Massenabnahme von Stählen und Nickelbasislegierungen bei Gegenwart von Sulfatmischungen in N_2 – 5 vol% O_2 bei 600 °C. Die höchste Massenzunahme wird unterhalb der $PbSO_4$-$ZnSO_4$-haltigen Sulfatablagerung beobachtet. Diese ist bei 600 °C schmelzflüssig

5 Experiments beneath heavy-metal rich sulfate melts

In order to study the effect of heavy-metalrich sulfates, experiments were carried out with low – and high alloy steels and also nickel-based alloys at 600 °C beneath four different sulfate mixtures containing $PbSO_4$ and/or $ZnSO_4$ (see Table 8).

In Fig. 37 the mass loss of the metallic material is shown for various sulfate mixtures, indicating a significant metal loss due to corrosion in the $PbSO_4$/$ZnSO_4$ containing salt. During the experiment at 600 °C this increase in corrosion is accompanied with melting of the salt. The highest metal loss is observed for the steels 10 CrMo 9 10 and X 20 CrMoV 12 1. The metal losses observed for the high alloy steel AC 66 and the nickel-based alloys are relatively small, whereas Alloy 625 exhibits the lowest mass loss. The morphology of the corrosive attack and also the reaction products are rather different, depending on the alloy.

The low alloy steel 10 CrMo 9 10 exhibits a thick and porous scale of Fe_2O_3 without any dissolved zinc and chromium, Fe_3O_4 was not detected. In the solidified sulfate melt on top of the scale, zinc-rich iron oxide precipitates are found without any chromium. Underneath the voluminous scale, FeS has formed, containing small amounts of dissolved chromium. The corrosion products on X 20 CrMoV 12 1 are shown in Fig. 38. In this case, also Fe_2O_3 precipitates are formed at the melt/gas interface, containing no chromium and various amounts of zinc. On top of the metal, a voluminous scale of Fe_2O_3 has formed, without any zinc and chromium. Underneath this scale, pits filled with a layered corrosion product are growing into the metal, consisting of chromium-rich oxides with more or less zinc and iron, obviously (Zn, Fe)(Cr, Fe)$_2O_4$. These layers are alternating with solidified K_2SO_4. At the metal/scale interface, iron- and chromium-sulfides are found. The corrosion products on the high alloy steel AC 66 are very different, no voluminous Fe_2O_3 scale is observed on the metal (Fig. 39), however, also oxide precipitates are found in the solidified melt on top of the scale, consisting of Fe_2O_3 and NiO with some dissolved zinc. The chromium content of the precipitates is undetectable at the former melt/gas phase boundary, however, at the melt/metal interface a small amount of chromium was detected. Also in this case pits are formed in the metal, filled with a layered corrosion product, consisting of chromium-rich phases containing zinc ($ZnCr_2O_4$) and small amounts of dissolved nickel and iron. At the metal/scale interface, sulfur was detected in combination with chromium.

The attack of the nickel-based alloys is quite low and the outer corrosion products are not very different from each

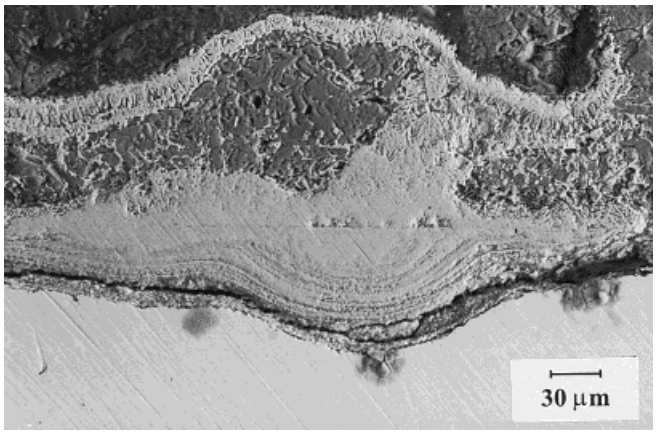

Fig. 38. SEM-image of a metallographic cross section of X 20 CrMoV 12 1 after corrosion in contact with a $CaSO_4$-K_2SO_4-Na_2SO_4-$PbSO_4$-$ZnSO_4$-salt mixture in N_2 – 5 vol.% O_2 at 600 °C. At the melt/gas interface, Fe_2O_3 precipitates are formed containing various amounts of zinc and no chromium. On top of the metal, a voluminous scale of Fe_2O_3 has formed, free of zinc and chromium. Underneath this scale, pits filled with a layered corrosion product are visible

Abb. 38. REM-Abbildung eines metallographischen Querschliffes von X 20 CrMo V 12 1 nach Korrosion in Kontakt mit einer $CaSO_4$-K_2SO_4-Na_2SO_4-$PbSO_4$-$ZnSO_4$-Salzmischung in N_2 – 5 vol.% O_2 bei 600 °C. An der Phasengrenze Schmelze/Gas bilden sich chromfreie Ausscheidungen von Eisenoxiden mit signifikanten Anteilen an Zink. Auf der metallsichen Matrix findet sich ebenfalls chromfreies, voluminöses Fe_2O_3 ohne gelöstes Zink. Unter dieser Schicht bilden sich Grübchen aus, die mit einem lagigen, chromreichen Korrosionsprodukt gefüllt sind

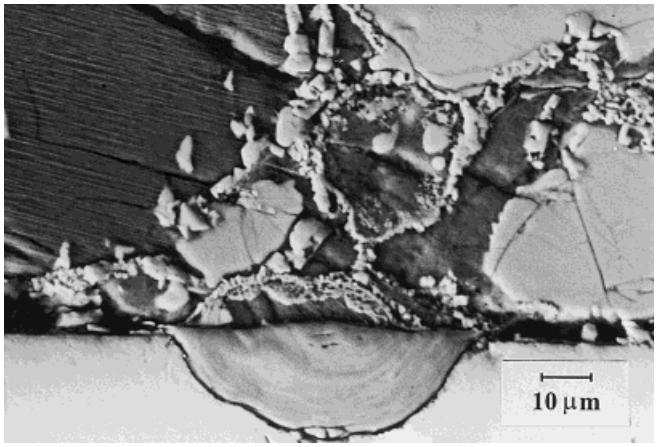

Fig. 39. SEM-image of a metallographic cross section of AC 66 after corrosion in contact with a $CaSO_4$-K_2SO_4-Na_2SO_4-$PbSO_4$-$ZnSO_4$-salt mixture in N_2 – 5 vol.% O_2 at 600 °C. At the melt/gas interface nickel- and iron-oxide precipitates are formed, containing various amounts of zinc and no chromium. Also pits filled with a layered, chromium-rich corrosion product are detected

Abb. 39. REM-Abbildung eines metallographischen Querschliffs von AC 66 nach Korrosion in Kontakt mit einer $CaSO_4$-K_2SO_4-Na_2SO_4-$PbSO_4$-$ZnSO_4$-Salzmischung in N_2 – 5 vol.% O_2 bei 600 °C. An der Phasengrenze Schmelze/Gas bilden sich chromfreie, nickel- und eisenhaltige Oxide mit unterschiedlichen Zinkgehalten. In der metallischen Matrix sind ebenfalls Grübchen mit einem lagigen, chromreichen Korrosionsprodukt zu finden

other. They consist of chromium-free iron-, nickel- and zinc-containing oxides, whereas some chromium is detected in precipitates close to the metal/melt interface. The inward growing corrosion products also exhibit pits, filled with a layered corrosion product. Comparing the three alloys, the chemistry of the layers is slightly different. In each case, K_2SO_4 is present within layers of chromium-rich oxides, containing variable amounts of zinc. In the case of Alloy 625, the iron content is quite low and no molybdenum was found all over the scale. The alloys 45 TM and 602 exhibit more iron in the corrosion product, due to the higher amount of iron in the alloy. The nickel content of the oxide is quite small for Alloy 625 and Alloy 602, however, in the case of 45 TM a reasonable amount of nickel is dissolved in the corrosion product as well as fine grained SiO_2.

In conclusion, if only a small amount of chromium is present in the alloy (10 CrMo 9 10), a thick and porous scale of Fe_2O_3 is formed, with FeS underneath. No pits with chromium-rich corrosion products are observed. If the chromium and nickel content of the alloy increases, pits are formed filled with chromium-rich corrosion products containing significant amounts of zinc along with chromium-free precipitates of iron- and nickel-oxides with dissolved zinc in the solidified melt. The amount of voluminous Fe_2O_3 decreases with decreasing iron content in the alloy. It is also interesting to note that in the case of chromium-containing iron-based alloys, the pits are covered with more or less Fe_2O_3.

The chemistry of a sulfate melt was described by *Lux* [17] as well as *Flood, Forland* and *Motzfeld* [18]. The melt contains oxide ions, generated by dissoziation of the sulfate ion:

$$SO_4^{2-} = SO_3 + O^{2-} \tag{23}$$

or in the special case of a Na_2SO_4-melt:

$$Na_2SO_4 = Na_2O + SO_3 \tag{24}$$

The basicity of a sulfate melt is given by the concentration of O^{2-}-ions and, therefore, it decreases with increasing $p(SO_3)$. In the presence of heavy-metal compounds like $ZnSO_4$ and $PbSO_4$ the activities of PbO and ZnO are much higher than those of Na_2O, CaO and K_2O, as shown in a previous publication [12]. The oxidation of the metal underneath the melt film occurs by oxygen molecules, stemming from the dissociation of the SO^{2-}_4-ion:

$$SO_4^{2-} = SO_2 + O^{2-} + 1/2\ O_2 \tag{25}$$

If the metal is oxidized, the activity of O^{2-} increases and the oxide is dissolved by basic dissolution. The experiments in the $ZnSO_4/PbSO_4$ containing melt have shown that the solubility of Fe_2O_3 and NiO appears to be quite high, compared with chromia. This is due to more acidic character of a melt containing heavy-metal sulfates according to their much higher dissociation pressures of SO_3. The solubility of chromia rapidly decreases with increasing acidic character of the melt [19] compared to Fe_2O_3 and NiO.

If the alloy contains only small amounts of chromium, Fe_2O_3 is dissolved in the melt and no passivation takes place:

$$Fe_2O_3 + O^{2-} = 2\ FeO_2^- \tag{26}$$

With time, the melt is saturated with dissolved iron oxide species and precipitation takes place in regions with a lower concentration of O^{2-}-ions, which is preferably the melt/gas interface. This precipitation leads to a concentration gradient of dissolved FeO_2^- within the melt film and, therefore, the metal is consumed. The corrosion product is a porous and voluminous Fe_2O_3 scale as observed in the experiment. If the chromium content of the alloy is too low, now chromium-rich corrosion products are able to form underneath the Fe_2O_3 scale.

The formation of FeS is closely related to the consumption of O_2 by oxidation of the metal and O^{2-} by dissolution of the oxide. According to reaction eqn. (18) this will lead to an increase in $p(SO_2)$ and, therefore, sulfides are stable in regions of low oxygen partial pressure and high sulfur activity, i.e. established at the metal/oxide interface by the reaction:

$$SO_2 = 1/2\ S_2 + O_2 \tag{27}$$

If the alloy contains medium amounts of chromium, zinc-rich chromium-containing corrosion products are formed in pits underneath a voluminous Fe_2O_3 scale. Obviously, chromium is enriched in the metal, close to the metal/scale interface by removal of iron according to reaction eqn. (26). In addition, no chromium-rich precipitates are observed in the melt. Hence, chromia is nearly insoluble in contact with the melt of this particular salt mixture, because $ZnCr_2O_4$ is formed by reaction:

$$ZnSO_4 + Cr_2O_3 = ZnCr_2O_4 + SO_3 \tag{28}$$

This spinel also contains some iron and, in the case of nickel-based alloy also small amounts of nickel. In the case of alloys with high chromium contents, only small amounts of precipitates are formed and no Fe_2O_3 scale. The chromium content is high enough to form chromia and, therefore, insoluble $ZnCr_2O_4$.

Considering the nickel-containing alloys, also NiO is found as precipitates in the sulfate melt, together with Fe_2O_3 and

dissolved zinc. The solubility of nickel in this sulfate mixture seems to be comparable to those of iron according to:

$$NiO + O^{2-} = NiO_2^{2-} \quad (29)$$

However, no voluminous scale of NiO was detected, which is due to the high amounts of chromium and the formation of a chromia scale on the nickel-based alloys.

6 Summary and conclusions

The paper presented the analysis of metallic materials, been in service in German waste incinerator plants for thousands of hours. The examinations have shown the formation of salt melts within the deposits and severe corrosion of the metallic materials underneath. The salt melts were identified as sulfates in contact with the flue gas and chlorides at the deposit/scale phase boundary. The chemical composition of the sulfate melts is within in the $CaSO_4$-K_2SO_4-Na_2SO_4 system, including heavy-metal compounds like $ZnSO_4$ and $PbSO_4$. The chloride melt is KCl-$ZnCl_2$ and also NaCl. The heavy-metal compounds decrease the melting point of the salt and a melt is formed.

A thermodynamic approach is given, in order to clarify the thermodynamic stability of sulfates with respect to chlorides under waste incineration conditions, i.e. HCl- and SO_2-containing gases. The heavy-metal sulfates form the less stable compounds and, therefore, they are converted to chlorides at relatively high $p(SO_2)$ in the presence of HCl(g). It was shown that sulfates are more stable at lower temperatures with respect to the corresponding chlorides and that heavy-metal chlorides are more stable than $CaCl_2$, NaCl and KCl and, therefore, converted to sulfates at relatively low temperatures. In HCl-containing gases a certain partial pressure of $PbCl_2$(g) and $ZnCl_2$(g) exists in equilibrium with the corresponding sulfate. This partial pressure decreases with decreasing temperature, i.e. dumping of the salt takes place by striking cooler metallic tubes. The calculations confirm the observation of heavy-metal chlorides present on superheater tubes and water walls in waste incineration plants.

Laboratory experiments were carried out in order to investigate the effect of molten $PbCl_2$, $ZnCl_2$ and of a KCl-$ZnCl_2$ mixture in the temperature range between 400–600 °C. Accelerated corrosion was observed for 10 CrMo 9 10 in the presence of $PbCl_2$ at 500 and 600 °C. A fluxing mechanism is proposed according to the occurrence of Fe_2O_3 precipitates at the melt/gas interface. The alloy AC 66 exhibit less corrosion due to the formation of insoluble $PbCrO_4$, accompanied by significant inward growth of spinel and metal-chlorides. In contact with $ZnCl_2$ accelerated corrosion was observed for 10 CrMo 9 10 at 600 °C, whereas at 500 °C inward diffusion of zinc into the oxide scale takes place and no accelerated corrosion was observed. Alloy AC 66 exhibits little corrosion and $ZnCr_2O_4$ is formed besides the formation of inward growing spinel and metal-chloride.

In contact with the KCl- $ZnCl_2$ melt, severe corrosion of the low alloy 2.25Cr-1Mo-steel was observed at 300–400 °C and a complex multilayered scale is formed consisting of precipitates of $ZnFe_2O_4$ at the melt/scale phase boundary, a compact scale of Fe_2O_3 underneath and a potassium-rich oxide at the metal/scale interface. After an incubation time, Inconel 625 exhibits very high mass gains and a thick scale of a nickel, chromium- and molybdenum-containing corrosion product is formed.

In addition, the corrosion of steels and nickel-based alloys was studied beneath a $CaSO_4$-K_2SO_4-Na_2SO_4-$PbSO_4$-$ZnSO_4$-mixture at 600 °C. In contact with the sulfate melt, also accelerated corrosion was observed, whereas the nickel-based alloy behave rather resistant. The experiments clearly show the corrosive effect of a molten $CaSO_4$-K_2SO_4-Na_2SO_4-$PbSO_4$-$ZnSO_4$-salt mixture in the corrosion of steels and nickel-based alloy at 600 °C. The corrosion products formed are oxide precipitates in the salt melt, containing zinc, iron and nickel, depending on the alloy. In the case of 10 CrMo 9 10 and X 20 CrMoV 12 1 an outer scale of zinc-free Fe_2O_3 is formed. Except on the 10 CrMo 9 10 alloy pits are formed in the other alloys containing layers of K_2SO_4 and chromium-rich corrosion products with significant amounts of zinc.

7 Acknowledgements

This work was carried out at the Department of Physical Chemistry of the Max-Planck-Institut für Eisenforschung GmbH, Düsseldorf, Germany. Many thanks are given to Prof. Dr. *H. J. Grabke* for the opportunity to work in his department and his ongoing interest in this topics of research. The author likes to thank also Mrs. *E. Strauch* for carrying out many of the experiments. Thanks is also given to the Max-Planck-Institut für Eisenforschung GmbH for the possibility to use the scientific equipment and the personal staff. The financial support from the DFG (Deutsche Forschungsgemeinschaft) is gratefully acknowledged.

8 References

[1] Statistisches Bundesamt Wiesbaden (1992), Statistik der öffentlichen Abfallbeseitigung von 1990.
[2] Richtlinien VDI 2114, (1992).
[3] *I. G. Wright, H. H. Krause:* ASME Research Report, CRTD – Vol. 38, The American Soc. of Mech. Eng., New York, (1996).
[4] *G. Sorrell:* Materials at High Temperatures *14* (1997) 207.
[5] *D. A. Vaughan, H. H. Krause, W. K. Boyd:* Materials Performance *14* (1975) 16.
[6] *D. A. Vaughan, H. H. Krause, W. K. Boyd:* Ash Deposits and Corrosion Due to Impurities in Combustion Gases. Hemisphere Publishing Corp., Washington D.C. (1977).
[7] *E. Reese, H. J. Grabke:* Materials and Corrosion *43* (1992) 547.
[8] *E. Reese, H. J. Grabke:* Materials and Corrosion *44* (1993) 41.
[9] *Y. Y. Lee, M. J. McNallan:* Metallurg. Trans. *18A* (1987) 1099.
[10] *M. Spiegel, H. J. Grabke:* Materials and Corrosion *46* (1995) 121.
[11] *M. Spiegel:* Materials at High Temperatures *14* (1997) 221.
[12] *M. Spiegel, H. J. Grabke:* Materials and Corrosion *47* (1996) 179.
[13] *N. Otsuka, A. Natori, T. Kudo, T. Imoto:* Paper No. 289, CORROSION/93, NACE International, Houston, Texas, (1993).
[14] *Y. Kawahara:* Materials at High Temperatures *14* (1997) 261.
[15] Stahl-Eisen-Liste, Verlag Stahleisen, Düsseldorf (1990).
[16] *H. Schmalzried:* Werkst. Korros. *22* (1971) 371.
[17] *H. Lux:* Z. Elektrochem. angew. phys. Chem. *45* (1935) 303.
[18] *H. Flood, T. Forland, K. Motzfeld:* Acta chem. Scand. *6* (1952) 257.
[19] *R. A. Rapp:* Corrosion NACE *42* (1986) 568.

(Received: August 25, 1998) W 3333